

A direct technique for the homogenization of periodic beam-like structures by transfer matrix eigen-analysis

Abstract

To homogenize lattice beam-like structures, a direct approach based on the matrix eigen- and principal vectors of the state transfer matrix is proposed and discussed. The Timoshenko couple-stress beam is the equivalent continuum medium adopted in the homogenization process. The girders unit cell transmits two kinds of bending moments: the first is generated by the couple of the axial forces acting on the section nodes, the other one is due to the moments directly applied at the node sections by the adjacent cells. This latter moment is modelled as the resultant of couple-stress. The main advantage of the method consists in to operate directly on the sub-partitions of the unit cell stiffness matrix. Closed form solutions for the transmission principal vectors of the Pratt and X-braced girders are also attained and employed to calculate the stiffnesses of the related equivalent beams. Unit cells having more complex geometries are analysed numerically. As a result, the principal vector problem is always reduced to the inversion of a well-conditioned (3×3) matrix employing the direct approach. Hence, no ill-conditioning problems, affecting all the known transfer methods, are present in the proposed method. Finally, comparing the predictions of the homogenized models with the finite element (f.e.) results of a series of girder, a validation of the homogenization method is performed.

Keywords

Pratt, X-braced and Warren girders – Beam like lattice – Timoshenko couple-stress beam – Homogenization.

Antonio Gesualdo^a
 Antonio Iannuzzo^a
 Giovanni Pio Pucillo^b
 Francesco Penta^b *

^a Dipartimento di Strutture per l'Ingegneria e l'Architettura, Università degli Studi di Napoli Federico II, Napoli, Italia. E-mail: gesualdo@unina.it, antonino.iannuzzo@unina.it

^b Dipartimento di Ingegneria Industriale, Università degli Studi di Napoli Federico II, Napoli, Italia. E-mail: gpucillo@unina.it, penta@unina.it

*Corresponding Author

<http://dx.doi.org/10.1590/1679-78254362>

Received August 04, 2017

In revised form October 09, 2017

Accepted December 01, 2017

Available online February 02, 2018

Notations

Latin letters:

\mathbf{A} stiffness matrix of the inner constrained unit cell

$\bar{\mathbf{A}}$ reduced stiffness matrix of the inner constrained unit cell

A_c, A_d chord and diagonal cross section areas

I_c, I_t, I_d chords, battens and diagonals second order central moment

\mathbf{d}_i dof's vector of the girder section i

\mathbf{f}_i vector of the alternative static quantities on the section i

\mathbf{G} state transfer matrix

$h = l_t$ girder height

\mathbf{K} unit cell stiffness matrices

l_c, l_d, l_t length of the unit cell chords, diagonal and battens

L girder span

M_i bending moment generated by the anti-symmetric axial forces on the girder section i

\hat{m}_i, \tilde{m}_i resultant of the nodal bending moments and difference between the top and bottom nodal bending moment on the section i

\hat{n}_i axial force on the girder section i

$\mathbf{P}_i^l, \mathbf{P}_i$ forces vector of the node i_l and of the section i

\bar{r} radius of curvature

\mathbf{S}_i state vector of the section i

\hat{u}_i axial displacement of the section i

u, v axial and transversal displacements of the equivalent beam cross section

u_i^l, v_i^l horizontal and vertical displacements of the node i_l

V_i shear force on the girder section i

Greek letters:

β_c, β_d axial stiffness parameters of chords and diagonals

Γ_b equivalent bending stiffness

Γ_p couple stress bending

Δ_p, Δ_a coefficient matrix determinants

δ_i^l, δ_i displacements vector of the node i_l and of the section i

ς, ξ dummy variables

η_c, η_d, η_t bending stiffness parameters of chords, diagonals and battens

θ_d slope angle of the girder diagonals

κ_a equivalent axial stiffness

κ_V equivalent shear stiffness

φ rotation of the equivalent beam cross section

φ_i^l rotation of the node i_l

$\hat{\varphi}_i, \tilde{\varphi}_i$ the symmetric and anti-symmetric parts of the nodal rotations of the girder section i

ψ_i rotation of the section i

Subscripts:

a, b, v axial, bending and coupled shear-bending force or displacement components

1 INTRODUCTION

In the last decades, a growing attention on periodic beam-like structures has been given by researchers and technicians operating in several engineering areas. In fact, this type of structures constitutes an optimal trade-off between strength and stiffness, on one side, and lightness, economy and manufacturing times, on the other. By these features they are frequently adopted in civil and industrial buildings, naval, aerospace and bridge constructions, material design and bio-mechanics (Salmon et al. (2008), Cao et al. (2007), Salehian et al. (2006), Cheng et al. (2013), Tej and Tejová (2014), Fillep et al. (2014), Zhang et al. (2016), El Khoury et al. (2011), Syerko et al. (2013), Ju et al. (2008)). In addition, the main component of the railway infrastructure, namely the track, has a periodic character and is often designed against the thermal buckling phenomenon assuming that rails, sleepers and fastenings are part of an infinitely long Vierendeel girder constrained to the ground by springs representative of the ballast actions. The importance of this topic is underlined by the fact that several publications have focused the issue, e.g. (Kerr and Zarembski (1981), Pucillo (2016), De Iorio et al. (2014a, 2014b, 2014c, 2017)).

The response of these types of structures to the service loads is usually analysed in a CAE environment. A f.e. discrete system models the girder-like structures and one of the solution methods for the structural framework problems is then applied to find the unknowns mechanical parameters.

If a considerable number of bays or unit cells composes the girder beam, to avoiding strong calculations charges especially during the preliminary design phase, it may be convenient to approximate its mechanical behaviour by a continuum 1-D model, whose properties come from those of the unit cell by a suitable homogenization method. Frequently, this kind of approach also offers the additional advantage of providing analytical closed form solutions for the problem at hand. Moreover, the continuous approximation may be employed as a means of transition to a coarser discrete system with a lower and more tractable set of kinematic and static unknowns.

To analyse correctly the in plane bending of periodic lattice structures, the classical continuum theory does not provide an acceptable approximation. In fact, several micropolar equivalent models have been reported for the analysis of planar lattices (Noor (1988), Bazant and Christensen (1972), Kumar and McDowell (2004), Bakhvalov and Panasenko (1989), Segerstad et al. (2009), Wang and Strong (1999), Warren and Byskov (2002), Onck (2002), Martinsson and Babuška (2007), Liu and Su (2009), Dos Reis and Ganghoffer (2012), Trovalusci et al. (2015), Bacigalupo and Gambarotta (2014), Hasanyan and Waas (2016)). While, the studies on the micro-polar models for analysing beam like lattices have not yet achieved the same advances. As far as the authors are aware, only few papers have specifically addressed this topic. In Noor and Nemeth (1980), Salehian and Inman (2010), a rational approach is presented where stiffness parameters of the effective continuum model were obtained using energy equivalence concepts. Nodal displacements of the unit cell were got in an approximated way by a Taylor expansion of the kinematical model of the substitute continuum. Then, the equivalent stiffnesses were derived by equating the potential and kinetic energies of a unit cell of the lattice beam to those of the equivalent continuum. This approach leads to two questionable stiffness couplings between the symmetric and anti-symmetric components of the shear stresses and between the bending and couple stress moments, making difficult the solution of the equilibrium equations of the equivalent beam, also for the simplest loading and constraint conditions. In Romanoff and Reddy (2014) the modified couple stress Timoshenko beam theory (Ma et al. (2008, Reddy (2011) is used to analyse the transversal bending of web-core sandwich panels. The equivalent polar bending stiffness was determined by invoking the spring analogy criterion. According to this rule, along the substitute beam, the ratio of the couple stress moment to the total bending moment is given by the ratio of the chords bending moment to the moment of the couple of axial forces acting in the panels faces. As it is shown in Gesualdo et al (2017b), this assumption unfortunately leads to an overestimation of the polar bending stiffness.

In this paper, the state transfer matrix eigen-analysis method is applied to evaluate the properties of the micropolar medium substituting a periodic beam-like structure. So far, the transfer matrix methods have been applied mostly for the dynamic analysis of repetitive or periodic structures (Mead (1970), Meirowitz and Engels (1977), Yong and Lin (1989), Langley (1996), i.e.). Just recently, it has also been used for the elasto-static analysis of prismatic, curved and pre-twisted repetitive beam like lattices made of pin-jointed bars (Stephen and Zhang (2004, 2006, Stephen and Ghosh, 2005). The main advantage of this method consists in evaluating both the Saint-Venant decay rates and the load transmission modes by carrying out an eigen-analysis of the unit cell transmission matrix \mathbf{G} . Although conceptually simple, its practical implementation is problematic, since the \mathbf{G} matrix is defective and ill-conditioned. Consequently, the Jordan block structure of \mathbf{G} is very difficult to be determined numerically.

Ill-conditioning, as noted in Zhong and Williams (1995), arises because the construction of the of the \mathbf{G} matrix, a (12×12) matrix for the simplest cases, requires the inversion of a partition of the stiffness matrix of the unit cell. Several alternative formulations have been proposed to avoid ill-conditioning in dynamic analysis (see ref. Stephen and Wang (2000) for a synthetic review). For the static problems, Stephen et al, instead, presented two related approaches, the force and displacement transfer methods, that achieve a better conditioning by analyzing the behavior of a lattice of n identical cells and lead to transfer matrices of reduced size, Stephen and Wang (2000).

The present paper introduces a direct technique approach for the homogenization of periodic beam-like lattice structures by the state transfer matrix eigen-analysis. The main advantage of the proposed method is that it operates directly on the sub-partitions of the unit cell stiffness matrix and, for this reason, all the drawbacks of the transfer methods till now proposed are avoided, see also Penta et al. (2017, 2018). For the simpler girder geometries, namely the Pratt and X-braced girders, closed form solutions for the unit cell force transmission modes are obtained and used to determine the stiffnesses of the equivalent beam. Doing so, neither approximations for the kinematical quantities nor subjective phenomenological assumptions on the inner moments are needed. The polar nature of the substitute beam, which is a Timoshenko couple-stress beam, is a direct consequence of the pure bending transmission mode components, since through the unit cell of the analysed girders two kinds of bending moments are transferred: one given by the axial forces, the other one stemmed by nodal moments.

The method can be easily extended also to more complex unit cell geometries composed of two or more bays. In these cases, eigen and principal vectors of \mathbf{G} must be determined numerically solving a linear algebraic system for the five kinematical quantities defining the deformed shape of the cell nodal sections. However, since the cell elastic responses are invariant for rigid translations, all the unit eigen-/principal vectors are defined up to the axial and transversal displacement components \hat{u} and v . Hence, the eigen/principal vector problem is always reduced to the inversion of a (3×3) matrix that is well conditioned and allows an accurate evaluation of the force transmission modes.

The real capability of the resulting equivalent beams in reproducing the behaviour of real discrete beam-like lattice structures is finally assessed performing some sensitivity analyses by a set of f.e. models. As a consequence, the accuracy of the results associate to the homogenized beams in a wide range of lattice parameters variation, satisfactorily validates the suggested direct technique.

2. EIGEN-ANALYSIS OF THE TRANSFER STATE MATRIX

To depict in a clear and concise manner the homogenization method we propose, some examples of immediate technical and engineering interest are examined in this section. Specifically, the Pratt girder problem is analysed in detail while the main results related to the X-braced girder are synthetically shown. The Vierendeel girder scheme, equally significant as the previous ones, is not explicitly considered since its solution can be obtained from those of the Pratt and X-braced girder by simply neglecting the stiffnesses of the diagonal rods. Finally, the problem of the Warren girder is also considered and the peculiar features of the method, making it more convenient when unit cell eigen and principal vectors can only be determined numerically, are highlighted.

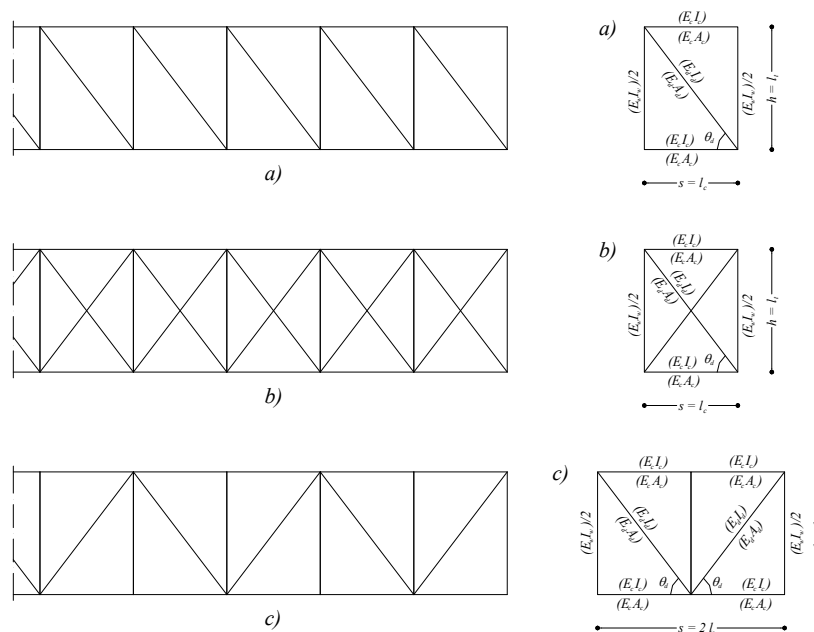


Figure 1: Beam-like lattices and their unit-cells: Pratt girder (a), X-braced girder (b) and Warren girder (c).

2.1 Pratt and X-braced girders

The unit cell of a Pratt girder is schematically represented in Figure 1. It is made up of two straight parallel chords rigidly connected both to the webs and to the diagonal. All the cell members are Bernoulli-Euler beams. The top and bottom chords have the same section whose area and second order central moment are denoted A_c and I_c , respectively. To simplify the analysis, we assume, that the girder transverse webs are axially inextensible. This is equivalent to supposing that transverse elongation among the chords is negligible during girder deformation. The cross-sectional area and the second order moment of the diagonal members are A_d and I_d . The second order

central moment of the transverse webs is indicated with I_w . However, to account for girder periodicity, the two vertical beams of the unit cell will have second order moment equal to the half part of I_w .

To identify any static or kinematical quantity related to the nodal section i of the girder, the sub-script i will be adopted, see Figure 2. To distinguish between the joints or nodes of the same section, the superscripts t or b are used, depending on whether the top or bottom chord is involved. Finally, in a coherent manner, top and bottom nodes of the section i are labelled i^t or i^b .

In what follows, we denote:

$$\delta_i^t = [u_i^t, v_i^t, \varphi_i^t]^T \quad \text{and} \quad \delta_i^b = [u_i^b, v_i^b, \varphi_i^b]^T \quad (1)$$

the displacement vectors of the joints i^t and i^b , where $u_i^{(\cdot)}$ and $v_i^{(\cdot)}$ are the displacement components of the joint $i^{(\cdot)}$ and $\varphi_i^{(\cdot)}$ is the rotation. Therefore, the displacement vector of the nodal section i is:

$$\delta_i = \left[\delta_i^{tT}, \delta_i^{bT} \right]^T.$$

Similarly, the nodal forces applied on the joints i^t and i^b of the cell are:

$$\mathbf{p}_i^t = \left[F_{ix}^t, F_{iy}^t, m_i^t \right]^T \quad \text{and} \quad \mathbf{p}_i^b = \left[F_{ix}^b, F_{iy}^b, m_i^b \right]^T \quad (2)$$

where $F_{ix}^{(\cdot)}$ and $F_{iy}^{(\cdot)}$ are respectively the axial and transversal force components and $m_i^{(\cdot)}$ the couple on the joint $i^{(\cdot)}$. Thus, the vector of the nodal forces acting on the section i of the girder is: $\mathbf{p}_i = \left[\mathbf{p}_i^{tT}, \mathbf{p}_i^{bT} \right]^T$.

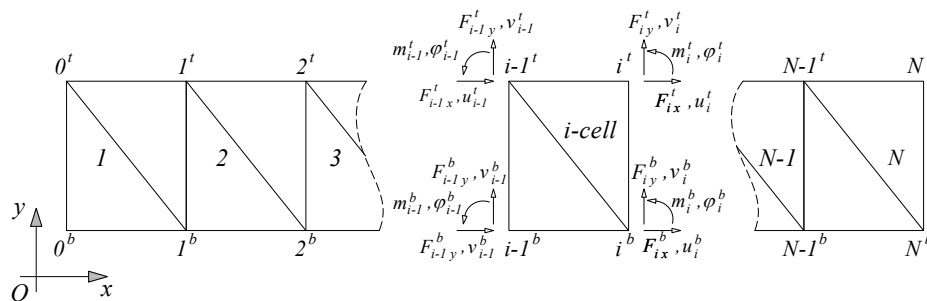


Figure 2: Unit cell nodes numbering with girder nodal inner forces and displacements

In what follows we assume that the positive components of \mathbf{p}_i are those acting according the reference axis on the right side of the cell (see Figure 2). Thus, the cell i , bounded by the sections $i-1$ and i respectively on the left and right sides will be loaded by the nodal force vectors $-\mathbf{p}_{i-1}$ and \mathbf{p}_i .

The Pratt cell stiffness matrix \mathbf{K} can be computed following the standard method adopted in the f.e. analysis, that is by additively assembling the stiffnesses of the beam components through the Boolean topological matrices. For our purposes, it is however more convenient to adopt alternative static and kinematic quantities to the standard ones of Figure 2 and eq. (1) and (2). More precisely, to identify the deformed configuration of a nodal section, we

use the mean axial displacement $\hat{u}_i = \frac{u_i^t + u_i^b}{2}$, the section rotation $\psi_i = \frac{u_i^b - u_i^t}{l_t}$ being l_t the web length, the trans-

verse displacement v and, finally, the symmetric and anti-symmetric parts of the nodal rotations of the section given respectively by:

$$\hat{\varphi}_i = \frac{\varphi_i^t + \varphi_i^b}{2} \text{ and } \tilde{\varphi}_i = \frac{\varphi_i^t - \varphi_i^b}{2}.$$

The static quantities conjugates of the previous kinematic variables are: the axial force $n_i = \frac{F_i^b + F_i^t}{2}$, the bending moment $M_i = (F_i^b - F_i^t)l_t$ generated by the anti-symmetric axial forces, the shear force $S_i = F_{iy}^t + F_{iy}^b$, the resultant of the section bending moments $\hat{m}_i = m_i^t + m_i^b$ and, finally, the difference between the same moments $\tilde{m}_i = m_i^t - m_i^b$.

The standard kinematic quantities δ_i can be expressed as functions of the new ones $\mathbf{d}_i = [\hat{u}_i \ \psi_i \ v_i \ \hat{\varphi}_i \ \tilde{\varphi}_i]$ through the matrix equation: $\delta_i = \mathbf{h}\mathbf{d}_i$,

being:

$$\mathbf{h} = \begin{bmatrix} 1 & -\frac{1}{2}l_t & 0 & 0 & 0 \\ 0 & 0 & 1 & 0 & 0 \\ 0 & 0 & 0 & 1 & 1 \\ 1 & \frac{1}{2}l_t & 0 & 0 & 0 \\ 0 & 0 & 1 & 0 & 0 \\ 0 & 0 & 0 & 1 & -1 \end{bmatrix}.$$

Denoting by $\mathbf{f}_i = [\hat{n}_i \ M_i \ S_i \ \hat{m}_i \ \tilde{m}_i]$ the vector of the alternative static quantities given by $\mathbf{f}_i = \mathbf{h}^T \mathbf{p}_i$, the unit cell stiffness equation in terms of the variables \mathbf{d} and \mathbf{f} can be written, in a partitioned form, as:

$$\begin{bmatrix} -\mathbf{f}_{i-1} \\ \mathbf{f}_i \end{bmatrix} = \begin{bmatrix} \Xi_{ll} & \Xi_{lr} \\ \Xi_{rl} & \Xi_{rr} \end{bmatrix} \begin{bmatrix} \mathbf{d}_{i-1} \\ \mathbf{d}_i \end{bmatrix}, \tag{3}$$

where subscript l and r are used to denote the left and right side of the unit cell and: $\Xi = \mathbf{H}^T \mathbf{K} \mathbf{H}$

is the cell stiffness matrix, \mathbf{H} being the (10×12) diagonal block matrix having as principal elements the (5×6) \mathbf{h} matrices.

The state vector \mathbf{s} of a nodal cross section of the girder consists of the displacements and forces vectors \mathbf{d} and \mathbf{f} . Hence, the state vectors of the end sections of the i cell are $\mathbf{s}_{i-1} = [\mathbf{d}_{i-1}^T, \mathbf{f}_{i-1}^T]^T$ and $\mathbf{s}_i = [\mathbf{d}_i^T, \mathbf{f}_i^T]^T$. They are related by the transfer matrix \mathbf{G} :

$$\mathbf{G}\mathbf{s}_{i-1} = \mathbf{s}_i, \tag{4}$$

or equivalently:

$$\begin{bmatrix} \mathbf{G}_{dd} & \mathbf{G}_{df} \\ \mathbf{G}_{fd} & \mathbf{G}_{ff} \end{bmatrix} \begin{bmatrix} \mathbf{d}_{i-1} \\ \mathbf{f}_{i-1} \end{bmatrix} = \begin{bmatrix} \mathbf{d}_i \\ \mathbf{f}_i \end{bmatrix} \tag{5}$$

In the simplest problems, where a nodal section contains only two nodes, the transfer matrix has size (12×12) .

As a first important consideration we can assert that the force transmission modes of the unit cell are given by the unit principal vectors of the \mathbf{G} matrix.

A state vector is transmitted unchanged or decays through the cell depending on whether its force components constitute a cross-sectional force or are self-equilibrating. This is equivalent to a scalar multiplication of the state vector, which leads immediately to an eigen-value problem. Indeed, by setting:

$$\mathbf{s}_i = \lambda \mathbf{s}_{i-1},$$

from eq. (4) the following eigen-value problem is derived:

$$(\mathbf{G} - \lambda \mathbf{I})\mathbf{s}_{i-1} = \mathbf{0} \tag{6}$$

The decay eigen-values occur as three reciprocal pairs depending on whether decay is from left to right, or vice-versa. The transmission eigen-value has unit value and a multiplicity of six, three of which pertain to the rigid body displacements, while the other three are related to the stress resultants of axial and shear forces and bending moment. Expanding the stiffness equation and rearranging the result according to eq. (5) we have:

$$\mathbf{G} = \begin{bmatrix} \mathbf{G}_{dd} & \mathbf{G}_{df} \\ \mathbf{G}_{fd} & \mathbf{G}_{ff} \end{bmatrix} = \begin{bmatrix} -\Xi_{lr}^{-1}\Xi_{ll} & -\Xi_{lr}^{-1} \\ \Xi_{rl} - \Xi_{rr}\Xi_{lr}^{-1}\Xi_{ll} & -\Xi_{rr}\Xi_{lr}^{-1} \end{bmatrix}$$

Since the sub-partitions of \mathbf{G} on the leading diagonal are independent of the Young modulus E while the blocks \mathbf{G}_{df} and \mathbf{G}_{fd} are proportional to E , \mathbf{G} is ill-conditioned Zhong and Williams (1995).

Ill conditioning can be avoided either solving the eigenvectors problem in closed form or recasting this problem in an alternative form that is non-pathological from a numerical point of view. Ill conditioning is automatically avoided on adopting the direct approach. Indeed, unit eigen- and principal vectors of the transfer matrix \mathbf{G} can be determined more simply operating directly on the unit cell stiffness matrix. If \mathbf{s}_e is a unit eigen-vector, its displacement and force sub vectors \mathbf{d}_e and \mathbf{f}_e are linked through the sub-partitions Ξ_{ij} of the stiffness matrix by virtue of the equations:

$$\begin{bmatrix} -\mathbf{f}_e \\ \mathbf{f}_e \end{bmatrix} = \begin{bmatrix} \Xi_{ll} & \Xi_{lr} \\ \Xi_{rl} & \Xi_{rr} \end{bmatrix} \begin{bmatrix} \mathbf{d}_e \\ \mathbf{d}_e \end{bmatrix}. \tag{7}$$

These latter relations follow from the stiffness equation, eq. (5), by imposing the conditions:

$$\mathbf{d}_{i-1} = \mathbf{d}_i = \mathbf{d}_e ; -\mathbf{f}_{i-1} = \mathbf{f}_i = \mathbf{f}_e.$$

Taking the second equation within eq. (3) and adding it to the first one, the vector \mathbf{f}_e is eliminated, since it results:

$$\mathbf{A} \mathbf{d}_e = \mathbf{0} , \tag{8}$$

where the \mathbf{A} matrix is obtained by adding the four sub-matrices Ξ_{ij} . For the Pratt girder case, by using the expressions of the sub matrix Ξ_{ij} given in Appendix 1, eq. (8) takes the form:

$$\begin{bmatrix} 0 & 0 & 0 & 0 & 0 \\ 0 & \beta_d \cos^2 \theta_d + 12 \eta_d \sin^4 \theta_d + 24 \eta_t & 0 & -12 \eta_d \sin^2 \theta_d - 24 \eta_t & 0 \\ 0 & 0 & 0 & 0 & 0 \\ 0 & -12 \eta_d \sin^2 \theta_d - 24 \eta_t & 0 & 24 \eta_c + 12 \eta_d + 24 \eta_t & 0 \\ 0 & 0 & 0 & 0 & 24 \eta_c + 4 \eta_d + 8 \eta_t \end{bmatrix} \begin{bmatrix} \hat{u}_e \\ \psi_e \\ \hat{v}_e \\ \hat{\varphi}_e \\ \tilde{\varphi}_e \end{bmatrix} = \begin{bmatrix} 0 \\ 0 \\ 0 \\ 0 \\ 0 \end{bmatrix} \tag{9}$$

in which the subscript e is adopted for the unknowns since they are eigenvector displacement components. By inspection of eq. (9), it is immediately recognized that the unit eigenvectors of \mathbf{G} are such that u_e and v_e are independent and indeterminate while $\psi_e = \hat{\varphi}_e = \tilde{\varphi}_e = 0$. In other words, they correspond to rigid translations of the unit cell along the axial and transversal directions and, for this reason, their force sub-vectors \mathbf{f}_e are the null vectors.

The principal vector \mathbf{s}_p of the \mathbf{G} matrix, generated by the state vector \mathbf{s}_v corresponding to a rigid transversal translation v , is defined by the condition: $\mathbf{G}\mathbf{s}_p = \mathbf{s}_p + \mathbf{s}_v$.

Equivalently, denoting by $\mathbf{d}_v = [0 \ 0 \ v \ 0 \ 0]^T$ the displacement sub-vector of \mathbf{s}_v , the displacement and force sub-vectors \mathbf{d}_p and \mathbf{f}_p of \mathbf{s}_p can be evaluated also solving the algebraic equations:

$$\begin{bmatrix} -\mathbf{f}_p \\ \mathbf{f}_p \end{bmatrix} = \begin{bmatrix} \Xi_{ll} & \Xi_{lr} \\ \Xi_{rl} & \Xi_{rr} \end{bmatrix} \begin{bmatrix} \mathbf{d}_p \\ \mathbf{d}_p + \mathbf{d}_v \end{bmatrix} \tag{10}$$

attained by substituting the conditions:

$$\mathbf{f}_i = -\mathbf{f}_{i-1} = \mathbf{f}_p$$

$$\mathbf{d}_{i-1} = \mathbf{d}_p \text{ and } \mathbf{d}_i = \mathbf{d}_p + \mathbf{d}_v$$

in the stiffness matrix equation, eq. (3). By adding term by term the two equations in (10), the successive condition for the displacement vector \mathbf{d}_p is deduced:

$$\mathbf{0} = \mathbf{A}\mathbf{d}_p + \mathbf{B}\mathbf{d}_v \tag{11}$$

where the matrix $\mathbf{B} = \Xi_{lr} + \Xi_{rr}$ is given by:

$$\mathbf{B} = \begin{bmatrix} 0 & 0 & 0 & 0 & 0 \\ -\frac{\beta_d \cos^2 \theta_d}{l_d \sin \theta_d} - 12 \frac{\eta_d}{l_d} \sin^3 \theta_d & \frac{1}{2} \beta_d \cos^2 \theta_d + 6 \eta_d \sin^4 \theta_d + 12 \eta_t & -\frac{\beta_d}{l_d} \cos \theta_d + 12 \frac{\eta_d}{l_d} \sin^2 \theta_d \cos \theta_d & 0 & 0 \\ 0 & 0 & 0 & 0 & 0 \\ 12 \frac{\eta_d}{l_d} \sin \theta_d & -6 \eta_d \sin^2 \theta_d - 12 \eta_t & -24 \frac{\eta_c}{l_c} - 12 \frac{\eta_d}{l_d} \cos \theta_d & 0 & 0 \\ 0 & 0 & 0 & 0 & 0 \\ -6 \eta_d \sin^2 \theta_d - 12 \eta_t & -6 \eta_d \sin^2 \theta_d & 0 & 0 & 0 \\ 12 \eta_c + 6 \eta_d + 12 \eta_t & 6 \eta_d & 0 & 0 & 0 \\ 2 \eta_d & 12 \eta_c + 2 \eta_d + 4 \eta_t & 0 & 0 & 0 \end{bmatrix}.$$

Thus, for the known term $-\mathbf{B}\mathbf{d}_v$ in eq. (11) it results:

$$-\mathbf{B} \mathbf{d}_v = \begin{bmatrix} 0 \\ -\frac{\beta_d}{l_d} \cos \theta_d + 12 \frac{\eta_d}{l_d} \sin^2 \theta_d \cos \theta_d \\ 0 \\ -24 \frac{\eta_c}{l_c} - 12 \frac{\eta_d}{l_d} \cos \theta_d \\ 0 \end{bmatrix} v. \quad (12)$$

Considering also the components of the \mathbf{A} matrix given in eq. (9), it can be inferred that the displacement vector \mathbf{d}_p is defined up to arbitrary rigid translations along the axial and transversal directions and that the antisymmetric rotation component $\hat{\varphi}_p$ of \mathbf{d}_p is equal to zero. Moreover, the symmetric rotation component $\hat{\varphi}_p$ and the section rotation component ψ_p are coupled by the second and fourth equations of eq. (11). They are quickly derived by using the following change of variables:

$$\zeta = \psi_p + \hat{\varphi}_p, \quad \xi = \psi_p - \hat{\varphi}_p. \quad (13)$$

Bearing in mind that $\sin^4 \theta_d = \sin^2 \theta_d (1 - \cos^2 \theta_d) = \sin^2 \theta_d - \sin^2 \theta_d \cos^2 \theta_d$, one gets from eq. (11), (12) and (9) the result:

$$\begin{aligned} \left[(\beta_d - 12 \sin^2 \theta_d \eta_d) \cos^2 \theta_d \right] \cdot \zeta + 2 \left[6 \sin^2 \theta_d (1 + \sin^2 \theta_d) \eta_d + \frac{1}{2} \cos^2 \theta_d \beta_d + 24 \eta_t \right] \cdot \xi &= -2 (\beta_d - 12 \sin^2 \theta_d \eta_d) \cos^2 \theta_d \frac{v}{l_c}; \\ \left[\cos^2 \theta_d \eta_d + 2 \eta_c \right] \cdot \zeta - \left[(1 + \sin^2 \theta_d) \eta_d + 2 \eta_c + 4 \eta_t \right] \cdot \xi &= -2 \frac{v}{l_c} \left[\cos^2 \theta_d \eta_d + 2 \eta_c \right]. \end{aligned}$$

Since in both the previous equations the coefficients of the unknown ζ are proportional to the known terms, for their solution it must be $\xi=0$ and $\zeta = \frac{v}{l_c}$. Thus, from eq. (13) it follows that $\hat{\varphi}_p = \psi_p = \frac{1}{2} \frac{v}{l_c}$, that is the principal state vector \mathbf{s}_p represents a rigid rotation of the cell cross section and its force sub-vector is the null vector. In the next, the state vector representing a rigid rotation is denoted by \mathbf{s}_φ and its displacement sub-vector is $\mathbf{d}_\varphi = [0 \quad \varphi \quad 0 \quad \varphi \quad 0]^T$.

The principal vector $\mathbf{s}_b = [\mathbf{d}_b^T \quad \mathbf{f}_b^T]^T$ generated by a rotation \mathbf{s}_φ is defined by the equation $\mathbf{G} \mathbf{s}_b = \mathbf{s}_b + \mathbf{s}_\varphi$. Its sub-vectors are evaluated by a procedure altogether similar to the one followed for \mathbf{s}_φ . The known term in equation (11) now becomes:

$$-\mathbf{B} \mathbf{d}_\varphi = \varphi \begin{bmatrix} 0 \\ 6 (\sin^4 \theta_d - \sin^2 \theta_d) \eta_d + \frac{1}{2} \beta_d \cos^2 \theta_d \\ 0 \\ 6 \eta_d \cos^2 \theta_d + 12 \eta_c \\ 2 \eta_d \end{bmatrix}$$

and also in this case, the displacement sub-vector is defined up to independent rigid translations along the axial and transversal directions. The anti-symmetric part of the nodal rotations is given by:

$$\hat{\varphi}_p = \frac{1}{2} \omega \varphi, \quad \text{with } \omega = \frac{\eta_d}{2 \eta_t + \eta_d + 6 \eta_c}.$$

Instead, the sectional and nodal rotation components ψ_p and $\hat{\varphi}_p$ are obtained employing the change of variable (13), achieving:

$$\psi_p = \hat{\varphi}_p = -\frac{1}{2}\varphi.$$

When the displacement sub-vector $\mathbf{d}_b = \left[0 \quad \frac{1}{2}\varphi \quad 0 \quad \frac{1}{2}\varphi \quad \frac{1}{2}\omega\varphi \right]^T$ and the vector $\mathbf{d}_b + \mathbf{d}_\varphi$ are applied respectively to the left and right cell sections, the typical cell deformed shape due to cell bending is obtained, see Figure 3.

Indeed, on substituting \mathbf{d}_b and $\mathbf{d}_b + \mathbf{d}_\varphi$ in place of \mathbf{d}_{i-1} and \mathbf{d}_i in the first equation of eq. (3), the force sub-vector is derived:

$$\mathbf{f}_b = \begin{bmatrix} 0 \\ \frac{1}{2}\beta_c \varphi \\ 0 \\ 2\eta_c \varphi + \eta_d (1 - \omega) \varphi \\ 0 \end{bmatrix}. \tag{14}$$

Shear force transfer properties of the Pratt unit cell are given by the \mathbf{G} principal vector $\mathbf{s}_V = \left[\mathbf{d}_V^T, \mathbf{f}_V^T \right]^T$ associated to the bending state vector \mathbf{S}_b .

The shear displacement \mathbf{d}_V can be evaluated in the same way as \mathbf{d}_b , namely adding the first and the second equation of eq. (3) after substitution of the positions:

$$\begin{aligned} \mathbf{d}_{i-1} &= \mathbf{d}_V & \mathbf{f}_{i-1} &= -\mathbf{f}_V \\ \mathbf{d}_i &= \mathbf{d}_V + \mathbf{d}_b & \mathbf{f}_i &= \mathbf{f}_V + \mathbf{f}_b. \end{aligned}$$

The algebraic system generated, whose coefficient matrix is still the \mathbf{A} matrix and the known terms vector, is:

$$\mathbf{f}_X = -\mathbf{B}\mathbf{d}_b + \mathbf{f}_b = \varphi \begin{bmatrix} 0 \\ \frac{1}{2}\beta_c + \frac{1}{4}\beta_d \cos^2\theta_d + 3\eta_d \sin^2\theta_d (\sin^2\theta_d - \omega - 1) \\ 0 \\ 8\eta_c + \eta_d (4 + 2\omega - 3\sin^2\theta_d) \\ (6\eta_c + \eta_d + 2\eta_t)\omega + \eta_d \end{bmatrix}.$$

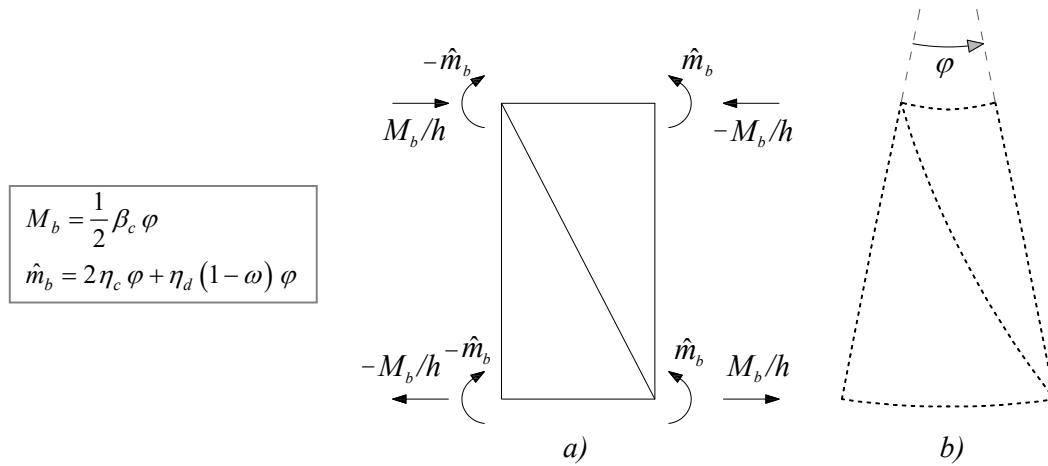


Figure 3: Bending principal vector force components (a) and unit cell deformed shape (b).

The anti-symmetric part of the nodal rotations $\tilde{\varphi}_V$ is immediately obtained, being uncoupled from the other components of \mathbf{d}_b (see eq. (9)):

$$\tilde{\varphi}_V = \frac{(6\eta_c + \eta_d + 2\eta_t)\omega + \eta_d}{4(2\eta_c + \eta_d + 2\eta_t)} \varphi = \frac{1}{2} \omega \varphi;$$

The translational components u_V and v_V of \mathbf{d}_V are indeterminate. The rotational components ψ_V and $\hat{\varphi}_V$ are given by the second and fourth equations of the algebraic system. These are solved by inverting the (2×2) sub-matrix of the non-zero coefficients of these equations and right-multiplying the result for the column vector formed by the second and fourth row of \mathbf{f}_X .

By this way, the expressions of ψ_V and $\hat{\varphi}_V$ are derived:

$$\psi_V = 12 \frac{\varphi}{\Delta_p} \left\{ (\eta_c + \eta_d + 2\eta_t) \left[\frac{\beta_c}{2} + \frac{1}{4} \beta_d \cos^2 \theta_d - 3\eta_d \sin^2 \theta_d (\cos^2 \theta_d + \omega) \right] + (2\eta_t + \eta_d \sin^2 \theta_d) \left[8\eta_c + \eta_d (3 \cos^2 \theta_d + 2\omega + 1) \right] \right\};$$

$$\hat{\varphi}_V = \frac{\varphi}{\Delta_p} \left\{ \left[12(2\eta_t + \eta_d \sin^2 \theta_d) \left[\frac{1}{2} \beta_c + \frac{1}{4} \beta_d \cos^2 \theta_d - 3\eta_d \sin^2 \theta_d (\cos^2 \theta_d + \omega) \right] + (\beta_d \cos^2 \theta_d + 12\eta_d \sin^4 \theta_d + 24\eta_t) \left[8\eta_c + \eta_d (3 \cos^2 \theta_d + 2\omega + 1) \right] \right\},$$

where

$$\Delta_p = (\beta_d \cos^2 \theta_d + 12\eta_d \sin^4 \theta_d + 24\eta_t) (24\eta_c + 12\eta_d + 24\eta_t) - (12\eta_d \sin^2 \theta_d + 24\eta_t)^2$$

is the determinant of the coefficients matrix.

The algebraic manipulations to determine the force sub-vector \mathbf{f}_v are cumbersome and time-consuming and, for brevity, they are omitted here. Besides, they are not necessary, since the transmitted shear force can be directly evaluated by analyzing the unit cell equilibrium.

The transmission mode of the axial force is finally given by the principal vector $\mathbf{s}_a = [\mathbf{d}_a^T, \mathbf{f}_a^T]^T$ corresponding to the axial translation unit eigenvalue. Its displacement sub-vector \mathbf{d}_a is defined by an equation analogous to eq.

(11) where in place of \mathbf{d}_v the axial displacement vector $\mathbf{d}_u = [u \ 0 \ 0 \ 0 \ 0]^T$ appears, while the force sub-vector \mathbf{f}_a is obtained by substituting \mathbf{d}_a and \mathbf{d}_u in eq. (3) in place of \mathbf{d}_{i-1} and \mathbf{d}_i . The components of \mathbf{d}_a and \mathbf{f}_a are: •

$$\mathbf{d}_a = \frac{u_a}{l_d \sin \theta_d} \begin{bmatrix} \# \\ 1 - 288 \eta_t \frac{(\eta_d \cos^2 \theta_d + 2 \eta_c)}{\Delta_a} \\ \# \\ 24 \eta_t \frac{(12 \eta_d \cos^2 \theta_d + \beta_d - 12 \eta_d) \cos^2 \theta_d}{\Delta_a} \\ 0 \end{bmatrix}, \tag{15}$$

$$\mathbf{f}_a = \frac{u_a}{l_d^2 \sin^2 \theta_d} \begin{bmatrix} 2 \beta_c + 288 \eta_t \frac{\beta_d (\eta_d + 2 \eta_c) \cos^2 \theta_d + 24 \eta_c \eta_d \sin^4 \theta_d}{\Delta_a} \\ 0 \\ 0 \\ 0 \\ 144 \frac{\beta_d \cos^2 \theta_d + 24 \eta_c \sin^2 \theta_d}{\Delta_a} \eta_t \eta_d l_d \sin \theta_d \end{bmatrix} \tag{16}$$

where the symbol # is adopted to denote indeterminate quantities. More details on the algebraic manipulations carried out to deduce eq. (14) and (15) are given in Appendix 2. §

Also for the X-braced girder, the eigen- and principal vectors analysis of the transmission matrix \mathbf{G} can be carried out in closed form. The sub-partitions of the base cell stiffness matrix are given in the Appendix 3. Adopting the same symbolism as the Pratt girder, only the main results that will be used for the girder homogenization are here reported:

- bending transmission mode:

$$\mathbf{d}_b = \varphi \begin{bmatrix} \# & -\frac{1}{2} & \# & -\frac{1}{2} & 0 \end{bmatrix}^T; \tag{17}$$

$$\mathbf{f}_b = \varphi \begin{bmatrix} 0 & \frac{1}{2} \beta_c & 0 & 2 \eta_c + 3 \eta_d & 0 \end{bmatrix}^T;$$

- sectional rotational component of the shear transmission mode:

$$\psi_V = \frac{12 \varphi}{\Delta_V} \left[(\eta_t + \eta_d + \eta_c) (\beta_c + \cos^2 \theta_d \beta_d + 12 \sin^2 \theta_d \cos^2 \theta_d \eta_d) + 4 (\eta_t + \eta_d \sin^2 \theta_d) (4 \eta_c + 3 \eta_d \cos^2 \theta_d + 3 \eta_{d1}) \right];$$

with $\Delta_V = 48 \left[(12 \eta_t + \beta_d \sin^4 \theta_d + 12 \eta_d \sin^4 \theta_d) (\eta_t + \eta_d + \eta_c) - 12 (\eta_t + \eta_d \sin^2 \theta_d)^2 \right];$

- axial force transmission mode:

$$\mathbf{d}_a = \begin{bmatrix} \# & 0 & \# & 0 & 0 \end{bmatrix}^T ;$$

$$\mathbf{f}_a = u_a \begin{bmatrix} \frac{2}{l_d^2 \sin^2 \theta_d} \beta_c + 2 \frac{\cos^2 \theta_d}{l_d^2 \sin^2 \theta_d} \beta_d + 24 \frac{\sin \theta_d}{l_d^2} \eta_d & 0 & 0 & 0 & 12 \frac{\sin \theta_d}{l_d} \eta_d \end{bmatrix}^T .$$

The analysis of the components of the \mathbf{f}_b vectors given in eq. (14) and (17) reveals that two bending moments are transferred through the unit cell of the Pratt and X-braced girders. The first one is generated by the axial forces acting on the nodal cross sections, the other one is due to the moments applied at the joints of the unit-cell and is induced by the bending of chords and webs. In addition, in the case of the Pratt girder unit cell, when the diagonal is eliminated or equivalently $\beta_d = \eta_d = 0$, it results $\omega = 0$. Therefore $\tilde{\varphi}_p = 0$, and the top and bottom nodes of the cell rotate under bending exactly of the same angle of the cross section they belong to. In other words when $\beta_d = \eta_d = 0$, the cell transfers the bending moments without deformation of the transverse webs, a result already observed in Gesualdo et al (2017b) by numerical experimentation on Vierendeel unit cells.

In both kind of examined girders, axial force is transmitted together with anti-symmetric self-equilibrated moments applied at the nodes of each cell end-section. In addition, the unit cell of the Pratt girder deforms also with sectional and symmetric nodal rotations. These rotations are instead totally prevented in the X-braced girder due to symmetry of the unit cell.

2.2 Warren girder

The present approach can be also effectively adopted to analyse unit cells made up by more than one bay. To give an example we consider in this section the case of the Warren girder, whose unit cell is sketched in Figure 1c. To identify nodes and sections of the girder, we adopt a convention very similar to the one of the Pratt girder. The only difference is that here the sub-script c labels the kinematical and static quantities of the central or inner nodal section of the cell. Thus, the force and displacement vectors are respectively:

$$\mathbf{d} = \begin{bmatrix} \mathbf{d}_i^T & \mathbf{d}_c^T & \mathbf{d}_{i+1}^T \end{bmatrix}^T , \quad \mathbf{f} = \begin{bmatrix} \mathbf{f}_i^T & \mathbf{f}_c^T & \mathbf{f}_{i+1}^T \end{bmatrix}^T$$

As the Warren unit cell can be obtained by reflecting a Pratt unit cell, the stiffness matrix can be constructed starting from the one reported in Appendix 1 for the Pratt case. Furthermore, being the inner nodal section of the cell free of external load, the cell stiffness equation is:

$$\begin{bmatrix} \mathbf{f}_i \\ \mathbf{0} \\ \mathbf{f}_{i+1} \end{bmatrix} = \begin{bmatrix} \Xi_{ll} & \Xi_{lc} & \Xi_{lr} \\ \Xi_{cl} & \Xi_{cc} & \Xi_{cr} \\ \Xi_{rl} & \Xi_{rc} & \Xi_{rr} \end{bmatrix} \begin{bmatrix} \mathbf{d}_i \\ \mathbf{d}_c \\ \mathbf{d}_{i+1} \end{bmatrix} . \tag{18}$$

The second of previous equations allows expressing \mathbf{d}_c as function of \mathbf{d}_i and \mathbf{d}_{i+1} in the form:

$$\mathbf{d}_c = -\Xi_{cc}^{-1} \Xi_{cl} \mathbf{d}_i - \Xi_{cc}^{-1} \Xi_{cr} \mathbf{d}_{i+1}$$

When previous result is substituted in the first and third equation of eq. (18), the \mathbf{d}_c vector is eliminated and the stiffness equation can be written as:

$$\begin{bmatrix} \mathbf{f}_i \\ \mathbf{f}_{i+1} \end{bmatrix} = \begin{bmatrix} \Xi_{ll} & \Xi_{lr} - \Xi_{lc} \Xi_{cc}^{-1} \Xi_{cl} \\ \Xi_{rl} - \Xi_{rc} \Xi_{cc}^{-1} \Xi_{cr} & \Xi_{rr} \end{bmatrix} \begin{bmatrix} \mathbf{d}_i \\ \mathbf{d}_{i+1} \end{bmatrix} \tag{19}$$

The reduced stiffness matrix of eq. (19) has some properties that make very simple the numerical searching of the principal vectors of the \mathbf{G} matrix. To highlight them, preliminary we observe that rigid translations of the cell do not produce any force and moment on the cross sections. This implies that the algebraic sums respectively of the first and the sixth columns and of the third and the height columns of the reduced stiffness matrix must give

the null vectors. Being the matrix symmetric, also the sum of its first and sixth rows and third and eight rows will give the null vectors. Therefore, the \mathbf{A} matrix of the principal vector problem, being extracted by adding the four contiguous (5×5) sub-partitions of the condensed stiffness matrix in eq. (19), will systematically have the first and third columns and the first and third rows zero-filled. This is true also when the cell has only one bay, as the Pratt and X-braced girders of previous section. Furthermore, the \mathbf{A} matrix can be viewed as the stiffness matrix of the plane elastic system obtained from the unit cell by introducing the inner constraint conditions:

$$\mathbf{d}_i = \mathbf{d}_{i+1} = \mathbf{d}$$

and, for this reason, it is semi-positive definite. It exhibits always the following symmetric structure:

$$\mathbf{A} = \begin{bmatrix} 0 & 0 & 0 & 0 & 0 \\ 0 & a_{\psi\psi} & 0 & a_{\psi\hat{\varphi}} & a_{\psi\bar{\varphi}} \\ 0 & 0 & 0 & 0 & 0 \\ 0 & a_{\hat{\varphi}\psi} & 0 & a_{\hat{\varphi}\hat{\varphi}} & a_{\hat{\varphi}\bar{\varphi}} \\ 0 & a_{\bar{\varphi}\psi} & 0 & a_{\bar{\varphi}\hat{\varphi}} & a_{\bar{\varphi}\bar{\varphi}} \end{bmatrix}.$$

When also the dof's corresponding to the cell rigid longitudinal and transversal translations are constrained, the cell elastic behaviour will be totally defined by the stiffness matrix:

$$\bar{\mathbf{A}} = \begin{bmatrix} a_{\psi\psi} & a_{\psi\hat{\varphi}} & a_{\psi\bar{\varphi}} \\ a_{\hat{\varphi}\psi} & a_{\hat{\varphi}\hat{\varphi}} & a_{\hat{\varphi}\bar{\varphi}} \\ a_{\bar{\varphi}\psi} & a_{\bar{\varphi}\hat{\varphi}} & a_{\bar{\varphi}\bar{\varphi}} \end{bmatrix}$$

which is positive definite and thus invertible.

In the case of the Pratt and X-braced unit cells, the algebraic sums of the indirect stiffnesses involving an anti-symmetric nodal rotation (i.e. the out-diagonal components in the last column of \mathbf{A}) are also zero, for symmetry reasons. When this happens, the antisymmetric rotation component can be determined straightforwardly being uncoupled from the other components of \mathbf{d}_p . To evaluate these latter components the (2×2) sub-matrix:

$$\hat{\mathbf{A}} = \begin{bmatrix} a_{\psi\psi} & a_{\psi\hat{\varphi}} \\ a_{\hat{\varphi}\psi} & a_{\hat{\varphi}\hat{\varphi}} \end{bmatrix}$$

must be inverted and this can be performed in closed form, hence avoiding altogether any ill-conditioning problem.

To compare the direct method with the classical one based on the \mathbf{G} matrix eigen-analysis and with those proposed in Stephen and Wang (2000), a Warren unit cell with the following properties is considered:

$$A_c = 3.5 \cdot 10^3 \text{ mm}^2 \quad I_c = 1.0 \cdot 10^7 \text{ mm}^4 \quad I_t = I_d = 5.0 \cdot 10^6 \text{ mm}^4 \quad A_d = 2.5 \cdot 10^3 \text{ mm}^2.$$

The corresponding $\bar{\mathbf{A}}$ matrix is:

$$\bar{\mathbf{A}} = \begin{bmatrix} 3.4576 \cdot 10^{11} & -9.2485 \cdot 10^9 & -4.1132 \cdot 10^9 \\ -9.2485 \cdot 10^9 & 4.0989 \cdot 10^9 & 4.4293 \cdot 10^9 \\ -4.1132 \cdot 10^9 & 4.4293 \cdot 10^9 & 3.6657 \cdot 10^{10} \end{bmatrix}.$$

Since the stiffness components of this matrix differ at most for two orders of magnitude, its condition number should be of order 10^{-2} . In fact, the MATLAB *rcond()* command, giving an estimate of the reciprocal condition number, for $\bar{\mathbf{A}}$ returns the value 9.0275E-02. The same command when executed on the \mathbf{G} matrix of the same cell gives the value 1.3865E-24.

In Table 1 the *rcond()* outputs obtained for the displacement and force transfer matrices \mathbf{S} and \mathbf{M} of Stephen and Wang (2000) for a series of girders composed of a number n of cell ranging between 5 and 10000 are listed.

From these results, it is clear that when the proposed method is adopted, the force transmission modes of the unit cell are determined by inversion of a matrix of reduced size that is well-conditioned and allows achieving the solutions with greater accuracy.

Table 1 – Warren girder force and displacement transfer matrices: reciprocals of the conditioning numbers

n	$rcond(\mathbf{M})$	$rcond(\mathbf{S})$
5	2.4912E-07	2.2011E-07
10	2.4912E-07	1.7593E-07
100	2.4912E-07	1.4352E-07
1000	2.4912E-07	1.4083E-07
10000	2.4090E-07	1.4057E-07

3. THE EQUIVALENT CONTINUUM

As equivalent continuum, the modified polar Timoshenko beam is adopted (Ma et al. (2008), Reddy (2011)). The displacements (U, V) of a point $P(x, y)$ of the beam (see Figure 4) are given by:

$$U = u(x) - y \cdot \varphi(x),$$

$$V = v(x),$$

where $u(x)$ and $v(x)$ denote respectively the longitudinal and transversal displacements of the beam axis and $\varphi(x)$ is the rotation of the cross section. The only not zero strains at P are the normal strain in the x direction:

$$\varepsilon_x = \frac{du}{dx} - y \frac{d\varphi}{dx},$$

the shear strain associated with the directions x and y :

$$\gamma_{xy} = \frac{dv}{dx} - \varphi(x),$$

and the curvature:

$$\chi_{xy} = \frac{1}{2} \frac{d\omega}{dx} = \frac{1}{4} \left(\frac{d\varphi}{dx} + \frac{d^2v}{dx^2} \right),$$

where $\omega = 1/2 \cdot (dv/dx + \varphi)$ is the rotation of an elementary neighbourhood of P in the x - y plane.

Denoting by $\delta(\cdot)$ the cinematically admissible variations of the strain components and by σ_x , τ_{xy} and m_{xy} respectively the normal, tangential and the couple stress acting on the beam cross section, the virtual strain energy or internal work can be expressed as:

$$\delta U = \int_l \int_A \left(\sigma_x \delta\varepsilon_x + \tau_{xy} \delta\gamma_{xy} + 2 m_{xy} \delta\chi_{xy} \right) dA dx =$$

$$= \int_l \left[N_x \frac{d\delta u}{dx} + M_x \frac{d\delta\varphi}{dx} + Q_x \left(\delta\varphi - \frac{d\delta v}{dx} \right) + \frac{1}{2} P_{xy} \left(\frac{d\delta\varphi}{dx} + \frac{d^2\delta v}{dx^2} \right) \right] dx,$$

where l is the beam length and A is the area of its cross section,

$$N_x = \int_A \sigma_x dA, \quad Q_x = -\int_A \tau_{xy} dA, \tag{20}$$

are the beam axial and shear forces, while:

$$M_x = -\int_A \sigma_x y dA \quad \text{and} \quad P_{xy} = \int_A m_{xy} dA. \tag{21}$$

are the Navier and polar bending moments, respectively. It is worth nothing that the dual shear deformation of Q_x is:

$$\gamma = -\gamma_{xy} = \varphi - \frac{dv}{dx}. \tag{22}$$

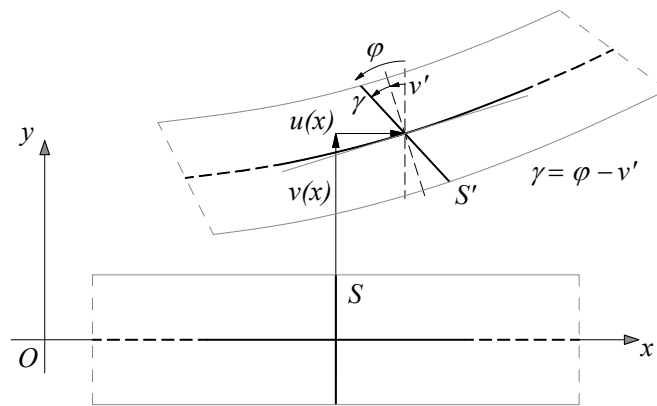


Figure 4: Kinematics of the Timoshenko beam

Under the assumption of homogeneous and isotropic linear elastic material, the stress-strain relationships are:

$$\sigma_x = E \varepsilon_x, \quad \tau_{xy} = G \gamma_{xy}, \quad m_{xy} = 2G \ell^2 \chi_{xy},$$

with E Young modulus, G tangential elasticity modulus and ℓ material length scale parameter. Substituting the previous constitutive relations in the expressions of the stress resultants, eq. (1) and (2), gives:

$$\begin{aligned} N_x &= A_{xx} \varepsilon_x, & Q_x &= D_Q \gamma, \\ M_x &= D_{xx} \frac{d\varphi}{dX}, & P_{xy} &= \frac{1}{2} S_{xy} \chi_{xy}, \end{aligned} \tag{23}$$

where A_{xx} and D_Q are respectively the axial and shear beam stiffnesses, $D_{xx} = EI$ is the bending stiffness, with I second order central moment of the beam cross section, and $S_{xy} = 4G\ell^2 A$ the couple stress bending stiffness.

The beam equilibrium equations can be derived equating the virtual internal work δU to the virtual work of the external loads, integrating by parts and taking into account the beam boundary conditions. For the simpler loading and constraint conditions, approximate solutions for these equations can be obtained by the Fourier series method (see ref. Reddy (2011) for more details).

4. EQUIVALENT STIFFNESSES

The homogenized beam stiffnesses can be determined by averaging over the unit cell length the cell responses under the load conditions defined by the force transmission principal vectors found in sec. 2. Thus, the equivalent axial stiffness of the homogenized beam is:

$$\kappa_a = \frac{\hat{n}_a}{\Delta u_a} = \frac{\hat{n}_a}{\hat{u}} \quad (24)$$

where \hat{n}_a is the axial component of the force sub-vector \mathbf{f}_a while $\Delta u_a = \hat{u}$ is the corresponding mean axial elongation of the unit cell.

The equivalent Navier bending stiffness Γ_b is calculated as the ratio of the bending moment M_b to the mean curvature $1/R$ of the cell. This latter is given by the relative rotations $\Delta\psi_b = \varphi$ of the cell end sections under bending divided by the cell length l_c (see Figure 3). Therefore, we have

$$\Gamma_b = M_b \cdot R = \frac{M_b l_c}{\varphi} \quad (25)$$

Polar bending stiffness Γ_p can be instead evaluated observing that, when the shear force is zero, from eq. (22) and (23) it follows:

$$\frac{d\varphi}{dX} = \frac{d^2 v}{dX^2}.$$

Hence, the polar and Navier moment of the homogenized beam make work by the same generalized strain, namely the beam curvature $\frac{d\varphi}{dX}$. For this reason, we can evaluate the polar bending stiffness as the ratio of the symmetric moment component of \mathbf{f}_b and the mean cell curvature:

$$\Gamma_p = \hat{m}_b R = \frac{\hat{m}_b l_c}{\varphi} \quad (26)$$

The shear principal vector \mathbf{s}_V is coupled with the pure bending one. The shear force component V is given by the subsequent condition:

$$-V l_c + M_b + \hat{m}_b = 0$$

which defines the in plane rotation equilibrium of the cell as reported in Figure 5. We recall that the displacement sub-vector \mathbf{d}_V is defined up to axial and transversal translations \hat{u} and v . The unit cell deformed shape due to shear and bending is also sketched in Figure 5 assuming that these latter quantities are equal to zero. In this case, the shear angle γ is equal to the average nodal section rotation $\bar{\psi}$ of the cell.

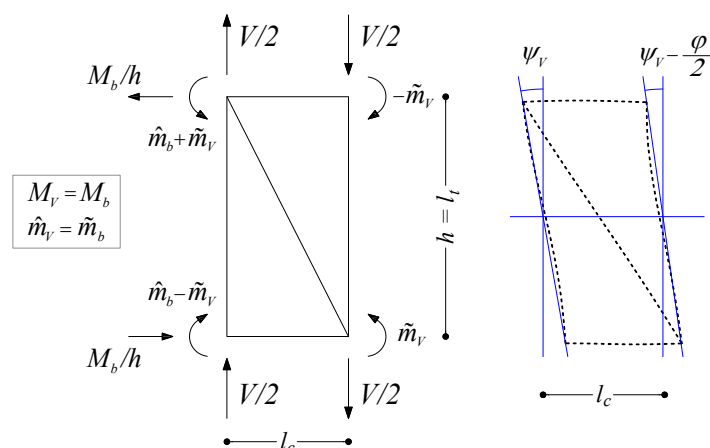


Figure 5: Coupled shear and bending principal vector force component and unit cell deformed shape

Bearing in mind the components of the displacement vector \mathbf{d}_v and $\mathbf{d}_v + \mathbf{d}_b$ defining the deformed configurations of the left and right sections of the cell under shear and bending, the following expression of $\bar{\psi}$ is easily deduced:

$$\bar{\psi} = \psi_v + \frac{1}{2}\psi_b.$$

Hence, the equivalent shear stiffness will be:

$$\kappa_V = \frac{V}{\gamma} = 2 \frac{M_b + \hat{m}_b}{l_c (2\psi_v + \psi_b)} \tag{27}$$

Axial and bending stiffnesses of the Pratt and X-braced girders, obtained by eq. (24), (26) and (26) and the results of sub-section 2.1, are reported in Table 2.

By inspection of these results it is deduced that Navier bending stiffnesses depend only on the chords axial stiffnesses and that, since bending of the X-braced unit cell occurs without deformation of the transvers webs, the equivalent polar bending stiffness of this girder is independent of η_t .

In addition, axial elongation of the Pratt unit cell is accompanied by rotations both of its joints and end sections. Consequently, its equivalent axial stiffness is dependent also on the bending stiffness of the chords and battens.

Table 2: Equivalent stiffnesses for Pratt and X braced girders

Bending stiffness:	
$\Gamma_b = \frac{1}{2}\beta_c l_c = \frac{1}{2}E_c A_c l_t^2$	
$\Gamma_p = 2\eta_c l_c + \gamma \eta_d l_d = 2E_c I_c + \gamma E_d I_d$	
with	
$\gamma = \begin{cases} 2 \cos \theta_d & \text{X-braced girder} \\ \frac{6E_c I_c \tan \theta_d + 2E_t I_t}{E_d I_d \sin \theta_d + 6E_c I_c \tan \theta_d + 2E_t I_t} \cos \theta_d & \text{Pratt girder} \end{cases}$	
Axial stiffness:	
$\kappa_a = 2 \frac{\beta_c l_c}{l_t^2} + \lambda_1 \frac{\beta_d}{l_t} + \lambda_2 \frac{\eta_d}{l_d} = 2E_c A_c + \lambda_1 E_d A_d + \lambda_2 \frac{E_d I_d}{l_d^2},$	
where	
$\lambda_1 = \begin{cases} 2 \cos^3 \theta_d & \text{X-braced girder} \\ \frac{288 E_t I_t}{\Delta_a l_t} \left(\frac{E_d I_d}{l_d} + 2 \frac{E_c I_c}{l_c} \right) \cos^3 \theta_d & \text{Pratt girder} \end{cases}$	
$\lambda_2 = \begin{cases} 24 \cos \theta_d \sin^2 \theta_d & \text{X-braced girder} \\ \frac{6912 E_t I_t E_c I_c}{\Delta_a l_t l_c} \cos \theta_d \sin^2 \theta_d & \text{Pratt girder} \end{cases}$	

The eqs. (24) - (27) completely define the elastic behaviour of the equivalent Timoshenko beam. The range of validity of these homogenized equations is analysed in the succeeding section on the basis of the numerical results of a sensitivity analysis.

5. VALIDATION STUDY

The equivalent beam model defined in Section 3, has been validated against a data set including information on the effects of the main geometrical parameters influencing the girder response. This set has been generated by f.e. solution of cantilevered and simply supported girders engendered by assembling Bernoulli-Euler beams and subjected to a unit vertical load applied respectively at the free end and at the midpoint.

The accuracy of the theoretical predictions has been quantified by the next non-dimensional measure of the homogenization error:

$$e\% = 100 \frac{\|\Delta \mathbf{v}\|}{\|\mathbf{v}_{FE}\|},$$

where \mathbf{v}_{FE} is the vector of the vertical displacements of the girder nodal sections derived through the f.e. analysis, $\Delta \mathbf{v}$ is the vector of the variations $\mathbf{v}_{hom} - \mathbf{v}_{FE}$, being \mathbf{v}_{hom} the vector of the vertical displacements of the corresponding homogenised beam evaluated at the nodal sections of the girders.

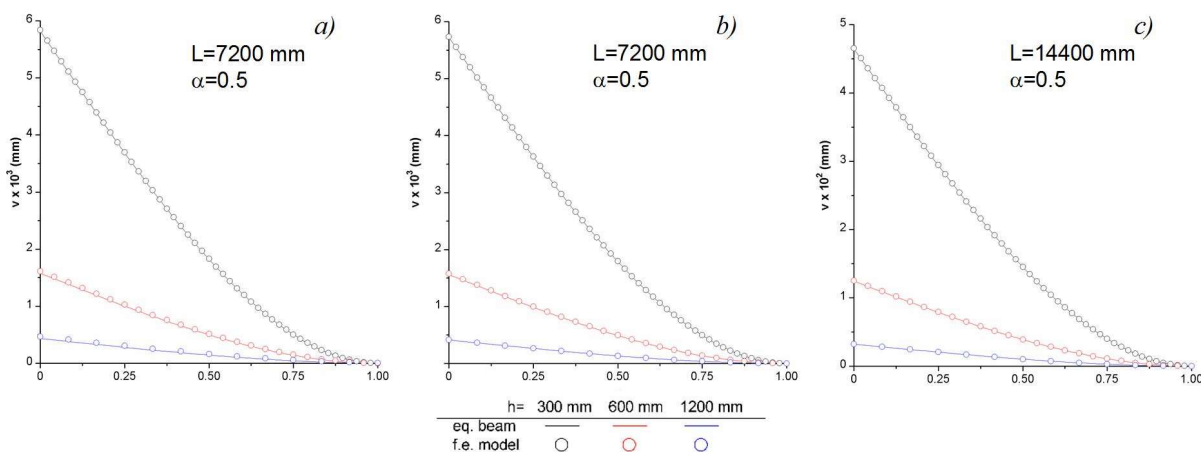


Figure 6: Deflections of Pratt (a), X-braced (b) and Warren (c) girders.

Furthermore, to have an additional measure of accuracy and to get also direct indications about the influence exerted on the model equilibrium shapes by the couple-stress bending stiffness, for each examined girder geometry the maximum displacement f of the equivalent model is compared with that f_{FE} of the corresponding f.e. model and the one \hat{f} of the Timoshenko (Cauchy) beam having the same bending and shear stiffness as the couple-stress equivalent beam.

Since, as a first approximation, the main parameter influencing the relative importance of the two bending moments acting on the girder cross section is the height h of the girder, in the first set of f.e. analysis the effects of the changes of this parameter have been considered. Under the assumption that both chords and webs have the same cross section, specifically HEA100, cantilever girder f.e. models having height $h=l_t=300, 600$ and 1200 mm, cell aspect ratios $\alpha = l_t/l_c = 0.5, 1$ and 2 and girder aspect ratio $\beta = L/l_t = 6, 12, 24$ and 48 , being L the girder span, have been examined. Previous values of h, α and β as well the cross sections properties were chosen to obtain girders geometries similar to those encountered in the practice of structural design.

In Figure 6, as an example, the deformed shapes of f.e. girders having cell-aspect ratio $\alpha=0.5$ are compared with those of the corresponding equivalent beams. In Tables 3, 4 and 5 for all the considered geometries respectively of Pratt, X-braced and Warren girders, the homogenization errors, the equivalent stiffnesses and the deflections f , f_{FE} and \hat{f} are listed.

From these results, it can be concluded that for the whole range of considered girder heights, to have accurate estimates of the girder displacements, it is necessary to take into account the bending stiffnesses of chords and webs by means of the couple stress stiffness of the equivalent beam. Furthermore, since small values of the homogenization error have been obtained for all the examined values of the cell shape ratio α , it is also clear that the homogenized model is able to offer insight into the effects of this parameter on the bending response of the girders.

A second series of girder models has been prepared to analyse the effects of the changes of diagonal cross-sectional area on the equivalent model accuracy, since the girder shear stiffness is strongly influenced by this geometric parameter. For these analysis, more stout girders under three points bending have been considered in order to highlight the shear properties effects in the girder response. For the chords of these models the standard HEA120 section has been chosen. Several back to back angles sections have been considered for the diagonals, while for the battens only the 80 x 8 back to back angle has been used.

Table 3: Pratt girders equivalent stiffnesses, deflections and homogenization errors as function of girder height and unit cell shape ratio.

	α	Γ_b	Γ_p	κ_V	f_{FE}	f	\hat{f}	e %
	[-]	[Nmm]	[Nmm]	[Nmm ⁻¹]	[mm]	[mm]	[mm]	[-]
h=300 mm	0.5	1.969E+13	1.740E+12	3.851E+08	5.840E-3	5.823E-03	6.356E-3	0.214
$\beta=24$	1	"	1.901E+12	2.334E+08	5.810E-3	5.791E-03	6.381E-3	0.261
	2	"	2.017E+12	1.092E+08	5.820E-3	5.791E-03	6.451E-3	0.335
h=600 mm	0.5	7.876E+13	1.740E+12	2.113E+08	1.610E-3	1.579E-03	1.648E-3	0.261
$\beta=12$	1	"	1.901E+12	1.737E+08	1.610E-3	1.583E-03	1.663E-3	0.620
	2	"	2.017E+12	8.580E+07	1.650E-3	1.621E-03	1.748E-3	1.455
h=1200 mm	0.5	3.150E+14	1.740E+12	1.701E+08	4.680E-4	4.344E-04	4.796E-4	0.700
$\beta=6$	1	"	1.901E+12	1.594E+08	4.640E-4	4.370E-04	4.853E-4	1.723
	2	"	2.017E+12	8.014E+07	5.170E-4	4.805E-03	5.746E-4	5.003

Table 4: X braced girders equivalent stiffnesses, deflections and homogenization errors as function of girder height and unit cell shape ratio.

α	Γ_b	Γ_p	κ_V	f_{FE}	f	\hat{f}	e %
[-]	[Nmm]	[Nmm]	[Nmm ⁻¹]	[mm]	[mm]	[mm]	[-]

h=300 mm	0.5	1.969E+13	2.082E+12	5.940E+08	5.557E-03	5.725E-03	6.343E-03	0.193
β=24	1	"	2.456E+12	4.033E+08	5.643E-03	5.634E-03	6.355E-03	0.212
	2	"	2.726E+12	1.974E+08	5.586E-03	5.582E-03	6.392E-03	0.091
h=600 mm	0.5	7.876E+13	2.082E+12	3.805E+08	1.574E-03	1.557E-03	1.618E-03	1.050
β=12	1	"	2.456E+12	3.322E+08	1.554E-03	1.553E-03	1.623E-03	0.157
	2	"	2.726E+12	1.665E+08	1.563E-03	1.568E-03	1.666E-03	0.458
h=1200 mm	0.5	3.150E+14	2.082E+12	3.298E+08	4.150E-04	4.138E-04	4.386E-04	0.118
β=6	1	"	2.456E+12	3.150E+08	4.140E-04	4.143E-04	4.406E-04	0.408
	2	"	2.726E+12	1.590E+08	4.280E-04	4.359E-04	4.855E-04	2.350

The f.e. results and the predictions of the homogenised model are compared in the diagrams of Figure 7, while in Table 6 the homogenization errors and the equivalent stiffnesses are reported. In all the examined cases the model predictions have resulted to be very close to the f.e. outcomes. Thus, the homogenized model is also able to predict the shear dominated girders responses with sufficient accuracy for practical applications.

Table 5: Warren girders equivalent stiffnesses, deflections and homogenization errors as function of girder height and unit cell shape ratio.

	α	Γ_b	Γ_p	κ_V	f_{FE}	f	\hat{f}	$e\%$
	[-]	[Nmm]	[Nmm]	[Nmm ⁻¹]	[mm]	[mm]	[mm]	[%]
h=300 mm	0.5	1.9689E+13	1.7604E+12	3.2517E+08	4.652E-02	4.6443E-2	5.0640E-2	0.177
β=24	1		1.9474E+12	1.7087E+08	4.614E-02	4.6078E-2	5.0720E-2	0.152
	2		2.0821E+12	6.4477E+07	4.594E-02	4.5917E02	5.1000E-2	0.056
h=600 mm	0.5	7.8758E+13	1.7604E+12	1.8875E+08	1.251E-02	1.2435E-2	1.2790E-2	0.565
β=12	1		1.9474E+12	1.2840E+08	1.245E-02	1.2441E-2	1.2860E-2	0.059
	2		2.0821E+12	5.0387E+07	1.254E-02	1.2588E-2	1.3210E-2	0.478
h=1200 mm	0.5	3.1503E+14	1.7604E+12	1.5493E+08	3.240E-03	3.2335E-3	3.3450E-3	0.170
β=6	1		1.9474E+12	1.1781E+08	3.250E-03	3.2604E-3	3.4040E-3	0.497
	2		2.0821E+12	4.6818E+07	3.360E-03	3.4410E-3	3.7750E-3	2.431

Table 6: Equivalent stiffnesses, deflections and homogenization errors as function of the diagonal geometry.

	diag-onal	Γ_b	Γ_p	κ_V	f_{FE}	f	\hat{f}	$e\%$
	[-]	[Nmm]	[Nmm]	[Nmm ⁻¹]	[mm]	[mm]	[mm]	[%]
Pratt girder	80 x 8	9.396E+13	2.702E+12	1.937E+08	-9.100E-5	-8.932E-5	1.013E-5	1.751

L=7200 mm	70 x 7	“	2.619E+12	1.500E+08	-9.400E-5	-9.197E05	1.068E-05	2.112	
	$\beta=12$	55 x 6	“	2.548E+12	1.035E+08	-9.900E-5	-9.714E05	1.176E-05	1.571
		30 x 6	“	2.505E+12	5.787E+07	-1.130E-5	-1.100E04	1.450E-05	2.021
X-braced girder	80 x 8	9.396E+13	2.918E+12	3.787E+08	-8.500E-5	-8.481E05	9.226E-05	0.763	
L=7200 mm	70 x 7	“	2.744E+12	2.910E+08	-8.600E-5	-8.633E05	9.513E-05	0.669	
	$\beta=12$	55 x 6	“	2.598E+12	1.979E+08	-8.900E-5	-8.923E05	1.009E-04	0.668
		30 x 6	“	2.512E+12	1.067E+08	-9.700E-5	-9.668E05	1.165E-04	0.424
Warren girder	80 x 8	9.396E+13	2.708E+12	1.441E+08	-6.660E-4	-6.675E04	7.120E-04	0.243	
L=14400 mm	70 x 7	“	2.621E+12	1.187E+08	-6.720E-4	-6.732E04	7.227E-04	0.193	
	$\beta=12$	55 x 6	“	2.548E+12	8.792E+07	-6.830E-4	-6.839E04	7.439E-04	0.211
		30 x 6	“	2.505E+12	5.298E+07	-7.110E-4	-7.100E04	7.979E-04	0.105

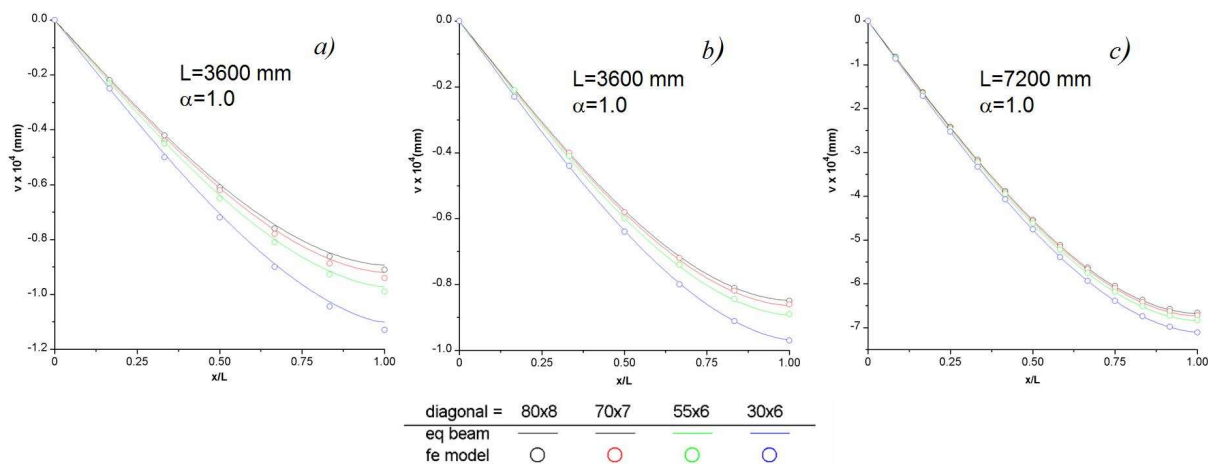


Figure 7: Deflections of Pratt (a), X-braced (b) and Warren (c) girders

6. CONCLUSION

A new procedure for homogenizing large repetitive beam-like structures is presented. Such a method is based on the analysis of the eigen- and principal vectors of the transfer state matrix of the unit cell. As a substitute medium, a Timoshenko polar beam is adopted. Differently from the approaches until now proposed, the polar character of the equivalent beam is not deduced by kinematical conjectures nor inspired by the micro-structure: it is a direct consequence of the pattern of the inner forces acting in the lattice when the pure bending mode of the cell is active.

The main advantage of the presented method is that it allows to operate directly on the sub-partitions of the unit cell stiffness matrix. For the simpler unit cells, as those of the Pratt and X braced girders, the method leads to closed form solutions for force transmission modes, that are then used to determine the stiffnesses of the corresponding equivalent beam. When the unit cell instead has a complex geometry and its transmission modes can be determined only numerically, it is shown that the method we propose has a very low computational cost, since the search of the transmission modes, reduces to the inversion of a (3 × 3) stiffness matrix, and has a higher accuracy, being this (3 × 3) matrix well-conditioned.

The results of a series of finite element simulations are presented for the deformed shapes of some simply supported and cantilever girders. In all the examined cases the predictions obtained with the homogenized models are in close agreement with the numerical f.e.m. outcomes.

The proposed homogenization technique is applicable in several field of structure or mechanical engineering interest. More specifically, it appears to be a serious candidate to analyse the buckling and post-buckling response of periodic beams infinitely long such as the railway track under thermal load (Pucillo (2016)) or to analyse the dynamic isolation of fragile goods in tall buildings (i.e. art objects, see Monaco et al. (2014); Gesualdo et al. (2014,

2017a). Its range of validity is bounded by the hypothesis of linear elasticity. Further research will thus be needed to extend the proposed method also in the elasto-plastic range whereas the response of the unit cell has to be analysed by approximated methods as those reported in Fraldi et al. (2010, 2014) and Cennamo et al. (2017).

References

Bacigalupo, A., Gambarotta, L., 2014. Homogenization of periodic hexa-and tetrachiral cellular solids, *Composite Structures*, 116:461-476.

Bakhvalov, N., Panasenko, G., 1989. Averaging processes in periodic media: mathematical problems in the mechanics of composite material, Kluwer Academic.

Bazant, Z., Christensen, M., 1972. Analogy between micropolar continuum and grid frameworks under initial stress, *International Journal of Solids and Structures*, 8(3):327-346.

Cao, J., Grenestedt, J.L., Maroun, W.J., 2007. Steel truss/composite skin hybrid ship hull. Part I: design and analysis, *Composites Part A: Applied Science and Manufacturing*, 38(7):1755-1762.

Cennamo, C., Gesualdo, A., Monaco, M., 2017. Shear plastic constitutive behaviour for near-fault ground motion, *ASCE Journal of Engineering Mechanics*, 143(9):04017086.

Cheng, B., Qian, Q., Sun, H., 2013. Steel truss bridges with welded box-section members and bowknot integral joints, Part I: linear and non-linear analysis, *Journal of Constructional Steel Research*, 80:465-474.

De Iorio, A., Grasso, M., Penta, F., Pucillo, G.P., Pinto, P., Rossi, S., Testa, M., Farneti, G., 2014a. Transverse strength of railway tracks: Part 1. Planning and experimental setup, *Frattura ed Integrità Strutturale*, 30:478-485.

De Iorio, A., Grasso, M., Penta, F., Pucillo, G.P., Rosiello, V., 2014b. Transverse strength of railway tracks: Part 2. Test system for ballast resistance in line measurement, *Frattura ed Integrità Strutturale*, 30:578-592.

De Iorio, A., Grasso, M., Penta, F., Pucillo, G.P., Rosiello, V., Lisi, S., Rossi, S., Testa, M., 2014c. Transverse strength of railway tracks: Part 3. Multiple scenarios test field, *Frattura ed Integrità Strutturale*, 30:593-601.

De Iorio, A., Grasso, M., Penta, F., Pucillo, G.P., Rossi, S., Testa, M., 2017. On the ballast-sleeper interaction in the longitudinal and lateral directions, *Proceedings of the Institution of Mechanical Engineers, Part F: Journal of Rail and Rapid Transit*, doi: <https://doi.org/10.1177/0954409716682629>.

Dos Reis, F., Ganghoffer, J.F., 2012. Construction of micropolar continua from the asymptotic homogenization of beam lattices, *Computers and Structures*, 112:354-363.

El Khoury, E., Messenger, T., Cartraud, P., 2011. Derivation of the young's and shear moduli of single-walled carbon nanotubes through a computational homogenization approach, *International Journal for Multiscale Computational Engineering*, 9(1):97-118.

Fillep, S., Mergheim, J., Steinmann, P., 2014. Microscale modeling and homogenization of rope-like textiles, *PAMM - Proceedings in Applied Mathematics and Mechanics*, 14(1):549-550.

Fraldi, M., Gesualdo, A., Guarracino, F., 2014. Influence of actual plastic hinge placement on the behavior of ductile frames, *Journal of Zhejiang University-Science A*, 15(7):482-495.

Fraldi, M., Nunziante, L., Gesualdo, A., Guarracino, F., 2010. On the bounding of multipliers for combined loading, *Proceedings of the Royal Society of London A: Mathematical, Physical and Engineering Sciences*, 466(2114):493-514.

Gesualdo, A., Iannuzzo, A., Monaco, M., Savino, M.T., 2014. Dynamic Analysis of Freestanding Rigid Blocks, in: B.H.V. Topping and P. Iványi (Eds.), *Civil-Comp Proceedings of the Twelfth International Conference on Computational Structures Technology*, Civil Comp Press, Kippen, Stirlingshire, U.K., (ISBN 978-1-905088-61-4).

Gesualdo, A., Iannuzzo, A., Monaco, M., Penta, F., 2017a. Rocking of a rigid block freestanding on a flat pedestal, *Journal of Zhejiang University-Science A*, 19(5):331-345.

Gesualdo, A., Iannuzzo, A., Penta, F., Pucillo, G.P., 2017b. Homogenization of a Vierendeel girder with elastic joints into an equivalent polar beam, *Journal of Mechanics of Materials and Structures*, 12(4):485-504.

Hasanyan, A.D., Waas, A.M., 2016. Micropolar constitutive relations for cellular solids, *Journal of Applied Mechanics*, 83(4):041001-1:10.

Ju, F., Xia, Z., Zhou, C., 2008. Repeated unit cell (RUC) approach for pure bending analysis of coronary stents, *Computer Methods in Biomechanics and Biomedical Engineering*, 11(4):419-431.

Kerr, A.D., Zarembski, A.M., 1981. The response equations for a cross-tie track, *Acta Mechanica*, 40(3-4):253-276.

Kumar, R.S., McDowell, D.L., 2004. Generalized continuum modeling of 2-D periodic cellular solids, *International Journal of Solids and Structures*, 41(26):7399-7422.

Langley, R.S., 1996. A transfer matrix analysis of the energetics of structural wave motion and harmonic vibration, *Proceedings of the Royal Society of London A: Mathematical, Physical and Engineering Sciences*, 452(1950):1631-1648.

Liu, S., Su, W., 2009. Effective couple-stress continuum model of cellular solids and size effects analysis, *International Journal of Solids and Structures*, 46:2787-2799.

Ma, H.M., Gao, X.L., Reddy, J.N., 2008. A microstructure-dependent Timoshenko beam model based on a modified couple stress theory, *Journal of the Mechanics and Physics of Solids*, 56(12):3379-3391.

Martinsson, P.G., Babuška, I., 2007. Mechanics of materials with periodic truss or frame micro-structures, *Archive for Rational Mechanics and Analysis*, 185(2):201-234.

Mead, D.J., 1970. Free wave propagation in periodically-supported infinite beams, *Journal of Sound and Vibration*, 13(2):181-197.

Meirowitz, L., Engels, R.C., 1977. Response of periodic structures by the z-transform method, *AIAA Journal*, 15(2):167-174.

Monaco, M., Guadagnuolo, M., Gesualdo, A., 2014. The role of friction in the seismic risk mitigation of freestanding art objects, *Natural Hazards*, 73(2):389-402.

Noor, A.K., 1988. Continuum modeling for repetitive lattice structures, *Applied Mechanics Reviews*, 41(7):285-296.

Noor, A.K., Nemeth, M.P., 1980. Micropolar beam models for lattice grids with rigid joints, *Computer Methods in Applied Mechanics and Engineering*, 21(2):249-263.

Onck, P.R., 2002. Cosserat modeling of cellular solids, *Comptes Rendus Mecanique*, 330(11):717-722.

Penta, F., Pucillo, G.P., Monaco, M., Gesualdo, A., 2017. Periodic beam-like structures homogenization by transfer matrix eigen-analysis: a direct approach, *Mechanics Research Communications*, 85:81-88.

Penta, F., Esposito, L., Pucillo, G. P., Rosiello, V., Gesualdo, A., 2018. On the homogenization of periodic beam-like structures, *Procedia Structural Integrity*, 8:399-409.

Pucillo, G.P., 2016. Thermal buckling and post-buckling behaviour of continuous welded rail track, *Vehicle System Dynamics*, 54(12):1785-1807.

Reddy, J.N., 2011. Microstructure-dependent couple stress theories of functionally graded beams, *Journal of the Mechanics and Physics of Solids*, 59(11):2382–2399.

Romanoff, J., Reddy, J.N., 2014. Experimental validation of the modified couple stress Timoshenko beam theory for web-core sandwich panels, *Composite Structures*, 111:130-137.

Salehian, A., Cliff, E.M., Inman, D.J., 2006. Continuum modeling of an innovative space-based radar antenna truss, *Journal of Aerospace Engineering*, 19(4):227-240.

Salehian, A., Inman, D.J., 2010. Micropolar continuous modeling and frequency response validation of a lattice structure, *ASME Journal of Vibration and Acoustics*, 132(1):011010.

Salmon, G.C., Johnson, J.E., Malhas, F.A., 2008. *Steel structures: design and behavior - (5th Edition)*, Prentice Hall.

Segerstad, P.H. AF, Toll, S., Larsson, R., 2009. Micropolar theory for the finite elasticity of open-cell cellular solids, *Proceedings of the Royal Society of London A: Mathematical, Physical and Engineering Sciences*, 465(2103):843–865.

Stephen, N.G., Ghosh, S., 2005. Eigenanalysis and continuum modelling of a curved repetitive beam-like structure, *International Journal of Mechanical Sciences*, 47(12):1854–1873.

Stephen, N.G., Wang, P.J., 2000. On transfer matrix eigenanalysis of pin-jointed frameworks, *Computers and Structures*, 78(4):603-615.

Stephen, N.G., Zhang, Y., 2004. Eigenanalysis and continuum modelling of an asymmetric beamlike repetitive structure, *International Journal of Mechanical Sciences*, 46(6):1213–1231.

Stephen, N.G., Zhang, Y., 2006. Eigenanalysis and continuum modelling of pre-twisted repetitive beam-like structures, *International Journal of Solids and Structures*, 43(13):3832–3855.

Syerko, E., Diskovsky, A.A., Andrianov, I.V., Comas-Cardona, S., Binetruy, C., 2013. Corrugated beams mechanical behavior modeling by the homogenization method, *International Journal of Solids and Structures*, 50(6):928-936.

Tej, P., Tejová, A., 2014. Design of an Experimental Prestressed Vierendeel Pedestrian Bridge Made of UHPC, *Applied Mechanics and Materials - Trans Tech Publications*, 587:1642-1645.

Trovalusci, P., Ostoja-Starzewski, M., De Bellis, M.L., Murrari, A., 2015. Scale-dependent homogenization of random composites as micropolar continua, *European Journal of Mechanics-A/Solids*, 49:396-407.

Wang, X.L., Strong, W.J., 1999. Micropolar theory for two-dimensional stresses in elastic honeycomb, *Proceedings of the Royal Society of London A: Mathematical, Physical and Engineering Sciences*, 455(1986):2091–2116.

Warren, W.E., Byskov, E., 2002. Three-fold symmetry restrictions on two-dimensional micropolar materials, *European Journal of Mechanics-A/Solids*, 21(5):779–792.

Yong, Y., Lin, Y.K., 1989. Dynamics of complex truss-type space structures, *AIAA Journal*, 28(7):1250–1258.

Antonio Gesualdo et al.

A direct technique for the homogenization of periodic beam-like structures by transfer matrix eigen-analysis

Zhang, S., Yin, J., Zhang, H. W., Chen, B.S., 2016. A two-level method for static and dynamic analysis of multilayered composite beam and plate, *Finite Elements in Analysis and Design*, 111:1-18.

Zhong, W.X., Williams, F.W., 1995. On the direct solution of wave propagation for repetitive structures, *Journal of Sound and Vibration*, 181(3):485-501.

Appendix 1 - Pratt girder: stiffness sub-matrices

The (5x5) blocks forming the leading diagonal of the Pratt unit cell stiffness matrix are given by:

$$\Xi_{xx} = \begin{pmatrix} 2 \frac{\beta_c}{l_d^2 \sin^2 \theta_d} + \frac{\beta_d \cos^2 \theta_d}{l_d^2 \sin^2 \theta_d} + 12 \frac{\eta_d \sin^2 \theta_d}{l_d^2} & \pm \left(\frac{1 \beta_d \cos^2 \theta_d}{2 l_d \sin \theta_d} + 6 \frac{\eta_d \sin^3 \theta_d}{l_d} \right) & \frac{\beta_d \cos \theta_d}{l_d^2 \sin \theta_d} - 12 \frac{\eta_d \sin \theta_d \cos \theta_d}{l_d^2} \\ \pm \left(\frac{1 \beta_d \cos^2 \theta_d}{2 l_d \sin(\theta_d)} + 6 \frac{\eta_d \sin^3 \theta_d}{l_d} \right) & \frac{\beta_c}{2} + \frac{1}{4} \beta_d \cos^2 \theta_d + 3 \eta_d \sin^4 \theta_d + 12 \eta_t & \pm \left(\frac{1 \beta_d \cos \theta_d}{2 l_d} - 6 \frac{\eta_d \sin^2 \theta_d \cos \theta_d}{l_d} \right) \\ \frac{\beta_d \cos \theta_d}{l_d^2 \sin \theta_d} - 12 \frac{\eta_d \sin \theta_d \cos \theta_d}{l_d^2} & \pm \left(\frac{1 \beta_d \cos \theta_d}{2 l_d} - 6 \frac{\eta_d \sin^2 \theta_d \cos \theta_d}{l_d} \right) & 24 \frac{\eta_c}{l_c^2} + \frac{\beta_d}{l_d^2} + 12 \frac{\eta_d \cos^2 \theta_d}{l_d^2} \\ \pm \left(-6 \frac{\sin \theta_d \eta_d}{l_d} \right) & -3 \eta_d \sin^2 \theta_d - 12 \eta_t & \pm \left(12 \frac{\eta_c}{l_c} + 6 \frac{\eta_d \cos \theta_d}{l_d} \right) \\ 6 \frac{\sin \theta_d \eta_d}{l_d} & \pm \left(3 \eta_d \sin^2 \theta_d \right) & -6 \frac{\eta_d \cos \theta_d}{l_d} \\ \pm \left(-6 \frac{\eta_d \sin \theta_d}{l_d} \right) & 6 \frac{\eta_d \sin \theta_d}{l_d} & \\ -3 \eta_d \sin^2 \theta_d - 12 \eta_t & \pm \left(3 \eta_d \sin^2 \theta_d \right) & \\ \pm \left(12 \frac{\eta_c}{l_c} + 6 \frac{\eta_d \cos \theta_d}{l_d} \right) & -6 \frac{\eta_d \cos \theta_d}{l_d} & \\ 8 \eta_c + 4 \eta_d + 12 \eta_t & \pm \left(-4 \eta_d \right) & \\ \pm \left(-4 \eta_d \right) & 4 \eta_d + 8 \eta_c + 4 \eta_t & \end{pmatrix},$$

with $x = l, r$ and $\eta_c = E_c I_c / l_c$, $\eta_d = E_d I_d / l_d$, $\eta_t = E_t I_t / l_t$, $\beta_c = E_c A_c l_t^2 / l_c$ and $\beta_d = E_d A_d l_t^2 / l_d$. For the components of Ξ_{xx} affected by the \pm , the upper sign is for $x = l$, the lower for $x = r$. Furthermore, for the upper and lower out-diagonal blocks it results:

$$\Xi_{lr} = \Xi_{rl}^T = \begin{pmatrix} -2 \frac{\beta_c}{l_d^2 \sin^2 \theta_d} - \frac{\beta_d \cos^2 \theta_d}{l_d^2 \sin^2 \theta_d} - 12 \frac{\eta_d \sin^2 \theta_d}{l_d^2} & \frac{1 \beta_d \cos^2 \theta_d}{2 l_d \sin \theta_d} + 6 \frac{\eta_d \sin^3 \theta_d}{l_d} & -\frac{\beta_d \cos \theta_d}{l_d^2 \sin \theta_d} + 12 \frac{\eta_d \sin \theta_d \cos \theta_d}{l_d^2} \\ -\frac{1 \beta_d \cos^2 \theta_d}{2 l_d \sin \theta_d} - 6 \frac{\eta_d \sin^3 \theta_d}{l_d} & -\frac{\beta_c}{2} + \frac{1}{4} \beta_d \cos^2 \theta_d + 3 \eta_d \sin^4 \theta_d & -\frac{1 \beta_d \cos \theta_d}{2 l_d} + 6 \frac{\eta_d \sin^2 \theta_d \cos \theta_d}{l_d} \\ -\frac{\beta_d \cos \theta_d}{l_d^2 \sin \theta_d} + 12 \frac{\eta_d \sin \theta_d \cos \theta_d}{l_d^2} & \frac{1 \beta_d \cos \theta_d}{2 l_d} - 6 \frac{\eta_d \sin^2 \theta_d \cos \theta_d}{l_d} & -24 \frac{\eta_c}{l_c^2} - \frac{\beta_d}{l_d^2} - 12 \frac{\eta_d \cos^2 \theta_d}{l_d^2} \\ 6 \frac{\eta_d \sin \theta_d}{l_d} & -3 \eta_d \sin^2 \theta_d & -12 \frac{\eta_c}{l_c} - 6 \frac{\eta_d \cos \theta_d}{l_d} \\ -6 \frac{\eta_d \sin \theta_d}{l_d} & 3 \eta_d \sin^2 \theta_d & 6 \frac{\eta_d \cos \theta_d}{l_d} \\ -6 \frac{\eta_d \sin \theta_d}{l_d} & -6 \frac{\eta_d \sin \theta_d}{l_d} & \\ -3 \eta_d \sin^2 \theta_d & -3 \eta_d \sin^2 \theta_d & \\ 12 \frac{\eta_c}{l_c} + 6 \frac{\eta_d \cos \theta_d}{l_d} & 6 \frac{\eta_d \cos \theta_d}{l_d} & \\ 4 \eta_c + 2 \eta_d & 2 \eta_d & \\ -2 \eta_d & 4 \eta_c - 2 \eta_d & \end{pmatrix}.$$

Appendix 2 - Pratt girder axial transmission mode components

The system of algebraic equations $\mathbf{A} \mathbf{d}_a = -\mathbf{B} \mathbf{d}_u$ giving the rotational components ψ_a , φ_{Sa} and φ_{Ea} of the displacement sub-vector \mathbf{d}_a , in explicit form becomes:

$$\begin{aligned} 0 &= 0, \\ (\beta_d \cos^2 \theta_d + 12 \eta_d \sin^4 \theta_d + 24 \eta_t) \psi_a - (12 \eta_d \sin^2 \theta_d + 24 \eta_t) \varphi_{Sa} &= \left(\frac{\beta_d \cos^2 \theta_d}{l_d \sin \theta_d} + 12 \frac{\eta_d \sin^3 \theta_d}{l_d} \right) u_a, \\ 0 &= 0, \\ - (12 \eta_d \sin^2 \theta_d + 24 \eta_t) \psi_a + (24 \eta_c + 12 \eta_d + 24 \eta_t) \varphi_{Sa} &= -12 \frac{\eta_d \sin \theta_d}{l_d} u_a, \\ (24 \eta_c + 4 \eta_d + 8 \eta_t) \varphi_{Ea} &= 0. \end{aligned} \tag{28}$$

The components of the corresponding sub-vector force $\mathbf{f}_a = [N_a \quad M_{ba} \quad V_a \quad m_{Sa} \quad m_{Ea}]^T$ transmitted by the cell are obtained by substituting \mathbf{d}_a and $\mathbf{d}_u + \mathbf{d}_a$ in place of \mathbf{d}_l and \mathbf{d}_r in the first equation of eq. (3):

$$\begin{aligned} N_a &= \left(2 \frac{\beta_c}{l_d^2 \sin^2 \theta_d} + \frac{\beta_d \cos^2 \theta_d}{l_d^2 \sin^2 \theta_d} + 12 \frac{\eta_d \sin^2 \theta_d}{l_d^2} \right) u_a - \left(\frac{\beta_d \cos^2 \theta_d}{l_d \sin \theta_d} + 12 \frac{\eta_d \sin^3 \theta_d}{l_d} \right) \psi_a + 12 \varphi_a \frac{\eta_d}{l_d} \sin \theta_d \\ M_{ba} &= \left(\frac{1}{2} \frac{\beta_d \cos^2 \theta_d}{l_d \sin \theta_d} + 6 \frac{\eta_d \sin^3 \theta_d}{l_d} \right) u_a - \left(\frac{1}{2} \beta_d \cos^2 \theta_d + 6 \eta_d \sin^4 \theta_d + 12 \eta_t \right) \psi_a + (6 \eta_d \sin^2 \theta_d + 12 \eta_t) \varphi_a \\ V_a &= \left(\frac{\beta_d \cos \theta_d}{l_d^2 \sin \theta_d} - 12 \frac{\eta_d \sin \theta_d \cos \theta_d}{l_d^2} \right) u_a - \left(\frac{\beta_d \cos \theta_d}{l_d} - 12 \frac{\eta_d \sin^2 \theta_d \cos \theta_d}{l_d} \right) \psi_a - \left(24 \frac{\eta_c}{l_c} + 12 \frac{\eta_d \cos \theta_d}{l_d} \right) \varphi_a \\ m_{Sa} &= -6 \frac{\sin \theta_d \eta_d u_a}{l_d} + (6 \eta_d \sin^2 \theta_d + 12 \eta_t) \psi_a - (12 \eta_c + 6 \eta_d + 12 \eta_t) \varphi_a \\ m_{Ea} &= 6 \frac{\sin \theta_d \eta_d u_a}{l_d} - 6 (\sin \theta_d)^2 \eta_d \psi_a + 6 \eta_d \varphi_a \end{aligned}$$

From the last equation in (28), it follows immediately that $\varphi_{Ea} = 0$. Furthermore, when the second and fourth equations of the system (28) are substituted respectively in the expressions of M_{ba} and m_{ba} , it is recognized that both these moments are equal to zero. Therefore, due to equilibrium, also the shear force component V_a must be null.

To get simpler expressions for the axial force N_a and for the rotations ψ_a and φ_{Sa} , we make the change of variable:

$$\psi = \frac{u_a}{l_d \sin \theta_d} + \psi_X \tag{29}$$

in eq. (28), deriving:

$$\begin{aligned} (\beta_d \cos^2 \theta_d + 12 \eta_d \sin^4 \theta_d + 24 \eta_t) \psi_X - (12 \eta_d \sin^2 \theta_d + 24 \eta_t) \varphi_S &= -24 \frac{\eta_t}{l_d \sin(\theta_d)} u_a \\ - (12 \eta_d \sin^2 \theta_d + 24 \eta_t) \psi_X + (24 \eta_c + 12 \eta_d + 24 \eta_t) \varphi_S &= 24 \frac{\eta_t}{l_d \sin \theta_d} u_a. \end{aligned} \tag{30}$$

Solutions of eq. (29) are:

$$\psi_X = -288 \eta_t \frac{(\eta_d \cos^2 \theta_d + 2 \eta_c)}{l_d \Delta_a \sin \theta_d} u_a$$

$$\varphi_a = 24 \eta_t \frac{(12 \eta_d \cos^2 \theta_d + \beta_d - 12 \eta_d) \cos^2 \theta_d}{l_d \Delta_a \sin \theta_d} u_a$$

where

$$\Delta_a = (\beta_d \cos^2 \theta_d + 12 \eta_d \sin^4 \theta_d + 24 \eta_t) (24 \eta_c + 12 \eta_d + 24 \eta_t) - (12 \eta_d \sin^2 \theta_d + 24 \eta_t)^2.$$

When the change of variable (29) is carried out in the first and last equations of (28) and previous solutions are then substituted, the following expressions of the axial force N_a and the self-equilibrated moment m_{Ea} :

$$N_a = \frac{2 \beta_c}{l_d^2 \sin^2 \theta_d} u_a + \frac{288 \eta_t}{\Delta_a l_d^2} \left[\frac{\beta_d (\eta_d + 2 \eta_c) \cos^2 \theta_d}{\sin^2 \theta_d} + 24 \eta_c \eta_d \sin^2 \theta_d \right] u_a,$$

$$m_{Ea} = 144 \eta_t \eta_d \frac{(\beta_d \cos^2 \theta_d + 24 \eta_c \sin^2 \theta_d)}{l_d \Delta_a \sin \theta_d} u_a,$$

are finally obtained.

Appendix 3 - X-braced girder: sub-partitions of the stiffness matrix

With the same notations as the Pratt girder of Appendix 1, the stiffness matrix sub-partitions of the X-braced girder are:

$$\Xi_{xx} = \begin{bmatrix} 2\frac{\beta_c}{l_d^2 \sin^2 \theta_d} + 2\frac{\beta_d \cos^2 \theta_d}{l_d^2 \sin^2 \theta_d} + 24\frac{\eta_d}{l_d^2} \sin^2 \theta_d & 0 & 0 \\ 0 & \frac{\beta_c}{2} + \frac{\beta_d}{2} \cos^2 \theta_d + 6\eta_d \sin^4 \theta_d + 12\eta_t & \pm \left(\frac{\beta_d}{l_d} \cos \theta_d - 12\frac{\eta_d}{l_d} \sin^2 \theta_d \cos \theta_d \right) \\ 0 & \pm \left(\frac{\beta_d}{l_d} \cos \theta_d - 12\frac{\eta_d}{l_d} \sin^2 \theta_d \cos \theta_d \right) & 24\frac{\eta_c}{l_c^2} + 2\frac{\beta_d}{l_d^2} + 24\frac{\eta_d}{l_d^2} \cos^2 \theta_d \\ 0 & 6\eta_d \sin^2 \theta_d - 12\eta_t & \pm \left(12\frac{\eta_c}{l_c} + 12\frac{\eta_d}{l_d} \cos \theta_d \right) \\ 12\frac{\eta_d}{l_d} \sin \theta_d & 0 & 0 \\ 0 & 12\frac{\eta_d}{l_d} \sin \theta_d & \\ 6\eta_d \sin^2 \theta_d - 12\eta_t & 0 & \\ \pm \left(12\frac{\eta_c}{l_c} + 12\frac{\eta_d}{l_d} \cos \theta_d \right) & 0 & \\ 8\eta_c + 8\eta_d + 12\eta_t & 0 & \\ 0 & 8\eta_d + 8\eta_c + 4\eta_t \end{bmatrix},$$

with $x=l,r$ and:

$$\Xi_{lr} = \Xi_{rl}^T = \begin{bmatrix} -2\frac{\beta_c}{l_d^2 \sin^2 \theta_d} - 2\frac{\beta_d \cos^2 \theta_d}{l_d^2 \sin^2 \theta_d} - 24\frac{\eta_d}{l_d^2} \sin^2 \theta_d & 0 & 0 \\ 0 & -\frac{\beta_c}{2} + \frac{\beta_d}{2} \cos^2 \theta_d + 6\eta_d \sin^4 \theta_d & -\frac{\beta_d}{l_d} \cos \theta_d + 12\frac{\eta_d}{l_d} \sin^2 \theta_d \cos \theta_d \\ 0 & \frac{\beta_d}{l_d} \cos \theta_d - 12\frac{\eta_d}{l_d} \sin^2 \theta_d \cos \theta_d & -24\frac{\eta_c}{l_c^2} - 2\frac{\beta_d}{l_d^2} - 24\frac{\eta_d}{l_d^2} \cos^2 \theta_d \\ 0 & -6\eta_d \sin^2 \theta_d & -12\frac{\eta_c}{l_c} - 12\frac{\eta_d}{l_d} \cos \theta_d \\ -12\frac{\eta_d}{l_d} \sin \theta_d & 0 & 0 \\ 0 & -12\frac{\eta_d}{l_d} \sin \theta_d & \\ -6\eta_d \sin^2 \theta_d & 0 & \\ 12\frac{\eta_c}{l_c} + 12\frac{\eta_d}{l_d} \cos \theta_d & 0 & \\ 4\eta_c + 4\eta_d & 0 & \\ 0 & 4\eta_c - 4\eta_d \end{bmatrix}.$$